Crustal Structure of the Ionian Basin and Eastern Sicily Margin: Results From a Wide-Angle Seismic Survey

David Dellong, Frauke Klingelhoefer, Heidrun Kopp, David Graindorge, Lucia Margheriti, Milena Moretti, Shane Murphy, Marc-André M-A Gutscher

AGU PUBLICATIONS

JGR

Journal of Geophysical Research: Solid Earth

RESEARCH ARTICLE
10.1002/2017JB015312

Key Points:
- We image a two-layered thin crust within the Ionian basin that we interpreted to be of probable oceanic origin
- The deep structure of the Malta Escarpment shows an abrupt crustal thinning zone that is interpreted to result from a transform origin of the margin
- The major tear fault accommodating the slab roll back of the subduction along the eastern Sicily margin was located along the Alfeo-Fault System

Supporting Information:
- Supporting Information S1

Correspondence to:
D. Dellong,
david.dellong@ifremer.fr

Citation:
Dellong, D., Klingelhoefer, F., Kopp, H., Graindorge, D., Margheriti, L., Moretti, M., et al. (2018). Crustal structure of the Ionian basin and eastern Sicily margin: Results from a wide-angle seismic survey. *Journal of Geophysical Research: Solid Earth*, *123*, 2090–2114. https://doi.org/10.1002/2017JB015312

Received 8 DEC 2017
Accepted 12 FEB 2018
Accepted article online 19 FEB 2018
Published online 11 MAR 2018

Crustal Structure of the Ionian Basin and Eastern Sicily Margin: Results From a Wide-Angle Seismic Survey

David Dellong[1,2], Frauke Klingelhoefer[2], Heidrun Kopp[3], David Graindorge[1], Lucia Margheriti[4], Milena Moretti[4], Shane Murphy[2], and Marc-Andre Gutscher[1]

[1]Laboratoire Géosciences Océan, IUEM, Université Brest, CNRS, Plouzané, France, [2]Géosciences Marines, Ifremer, Centre de Brest, Plouzané, France, [3]Geomar Helmholtz Centre for Ocean Research, Kiel, Germany, [4]Istituto Nazionale di Geofisica e Vulcanologia, Rome, Italy

Abstract In the Ionian Sea (central Mediterranean) the slow convergence between Africa and Eurasia results in the formation of a narrow subduction zone. The nature of the crust of the subducting plate remains debated and could represent the last remnants of the Neo-Tethys ocean. The origin of the Ionian basin is also under discussion, especially concerning the rifting mechanisms as the Malta Escarpment could represent a remnant of this opening. This subduction retreats toward the south-east (motion occurring since the last 35 Ma) but is confined to the narrow Ionian basin. A major lateral slab tear fault is required to accommodate the slab roll-back. This fault is thought to propagate along the eastern Sicily margin but its precise location remains controversial. This study focuses on the deep crustal structure of the eastern Sicily margin and the Malta Escarpment. We present two two-dimensional *P* wave velocity models obtained from forward modeling of wide-angle seismic data acquired onboard the R/V Meteor during the DIONYSUS cruise in 2014. The results image an oceanic crust within the Ionian basin as well as the deep structure of the Malta Escarpment, which presents characteristics of a transform margin. A deep and asymmetrical sedimentary basin is imaged south of the Messina strait and seems to have opened between the Calabrian and Peloritan continental terranes. The interpretation of the velocity models suggests that the tear fault is located east of the Malta Escarpment, along the Alfeo fault system.

1. Introduction

The Ionian basin, in the central-eastern Mediterranean Sea, is located between two major tectonic plates: Eurasia to the north and Africa/Nubia to the south. These two plates have been slowly converging during the last 80 Ma about 1 to 2 cm/year (Dercourt et al., 1986). This convergence leads to the formation of various subduction zones and back-arc basins in the Mediterranean by consuming the ancient Tethyan lithosphere that was formed during the Early Mesozoic (Dewey et al., 1989; Faccenna et al., 2001; Jolivet et al., 2015; Rosenbaum et al., 2002; van Hinsbergen et al., 2014). Since 35 Ma, roll-back of the NW dipping slab of Tethyan Oceanic lithosphere led to fragmentation of the Variscan basement blocks of the SW European margin, producing the Corsica-Sardinia block and the AlKaPeCa (Alboran, Kabylies, Peloritan, and Calabria) terranes (Bouillin, 1986; Lonergan & White, 1997; Malinverno & Ryan, 1986; Wildi, 1983). This roll-back to the SE reached the Ionian basin in the central Mediterranean since the late Miocene, thereby opening the Tyrrhenian back-arc basin (Figure 1b) (Jolivet et al., 2015; Prada et al., 2016; Stampfli et al., 2002; van Hinsbergen et al., 2014). Today these continental blocks (or microplates) are still moving toward the south-east (D'Agostino et al., 2011; Palano et al., 2012). A major lithospheric scale tear fault has been proposed to exist at the western edge of the Calabrian subduction zone, and this process was described as a "STEP" (Subduction Transform Edge Propagator) fault (Govers & Wortel, 2005). However, the exact position of the tear fault beneath the eastern Sicilian margin remains highly controversial (Argnani et al., 2009, 2016; Argnani & Bonazzi, 2005; Gallais et al., 2013; Gutscher et al., 2016, 2017; Orecchio et al., 2015; Polonia et al., 2011, 2016).

Today the Calabrian arc is considered to be one of the narrowest subduction zones in the world and a key area to understand the geodynamic evolution of the Mediterranean. Here the African plate (Ionian lithosphere) dips toward the NW underneath the Calabrian and Peloritan continental blocks. This region is also seismically and tectonically active, and several destructive events were recorded in historical times (e.g., M7.1 Messina 1908 and M7.5 Catania 1693; Figure 1).

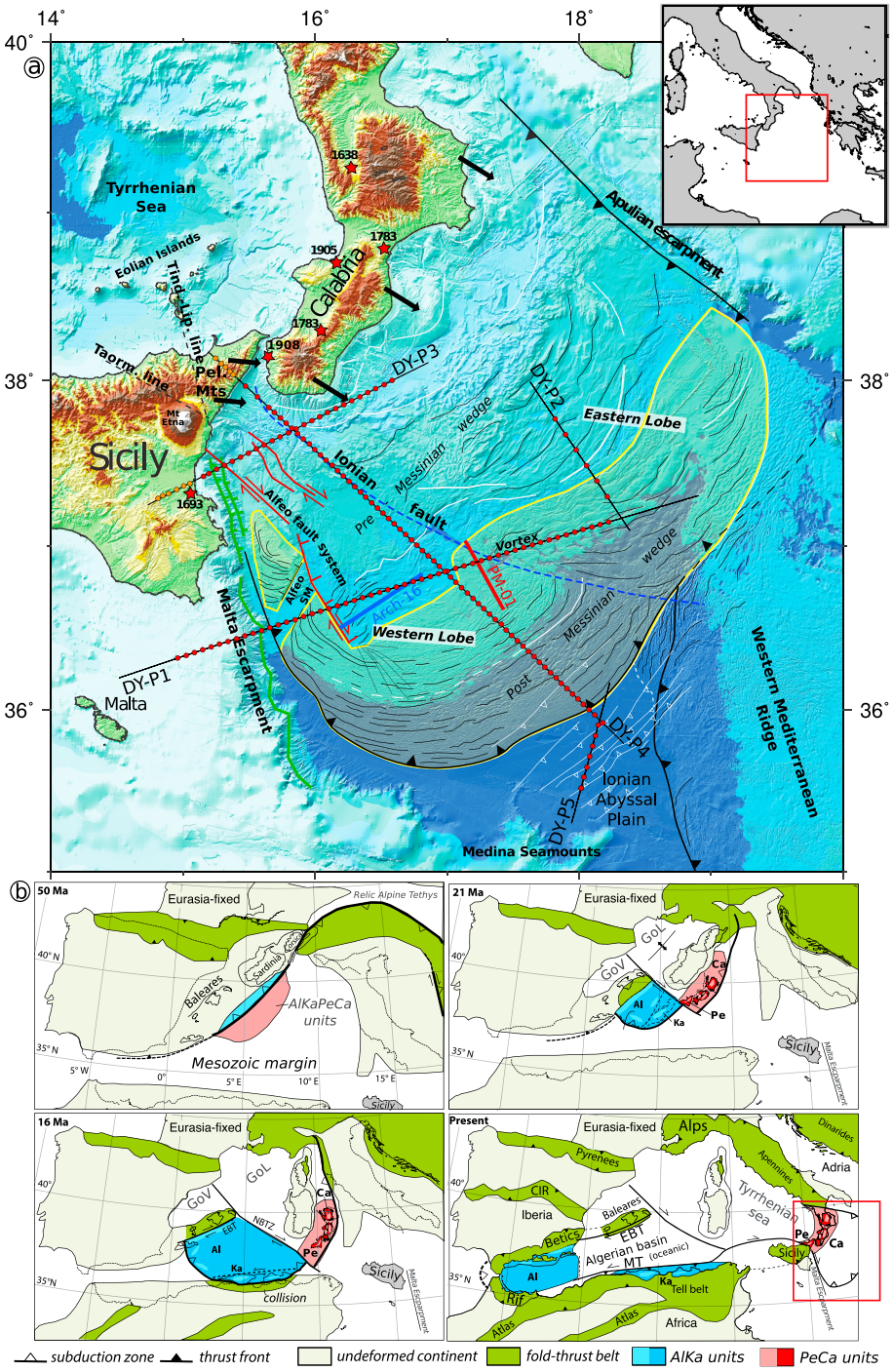

Figure 1. (a) Interpreted bathymetric map of the Ionian basin (modified from Gutscher et al., 2016). Superposed in black straight lines the wide-angle profiles from the DIONYSUS cruise with small red dots for the ocean bottom seismometer positions and orange dots for the land-stations position. The red stars show the position of major earthquakes and their corresponding dates. Reflection seismic profiles shown in Figure 10 of this paper are Arc-16 and PM-01 from respectively the Archimede (1997, R/V Le Nadir) and PrisMed (1993, R/V Le Nadir) cruises. The solid black arrows represent the interpreted motion of the Calabrian and Peloritan terranes from GPS data with a fixed Hyblean-Malta block (Palano et al., 2012). The yellow area represents the Messinian evaporite extent in the basin from morpho-bathymetric and seismic lines (Gutscher et al., 2017). The white lines in the Ionian Abyssal Plain are deep reverse faults (Gallais et al., 2011). (b) Reconstructions figures are modified from van Hinsbergen et al., 2014. Al = Alboran; Ca = Calabria; CIR = Central Iberian Ranges; EBD = Emile Baudot Transform; GoL = Gulf of Lion; GoV = Gulf of Valencia; Ka = Kabylides; NBTZ = North Balearic Transform Zone; Pe = Peloritan Mountains.

Despite decades of study, several important questions remain unanswered. Three of them will be addressed in this study. What is the direction of opening of the Ionian basin, thought to have occurred during Late Paleozoic or Early Mesozoic rifting (Catalano et al., 2001; Frizon de Lamotte et al., 2011)? What is the nature of the crust produced during the opening of the basin (Catalano et al., 2001; Dercourt et al., 1986; Frizon de Lamotte et al., 2011; Roure et al., 2012)? Finally, regarding the recent geodynamic (<10 Ma), where is the lateral slab tear fault located (Argnani et al., 2009; Gallais et al., 2013; Gutscher et al., 2016; Polonia et al., 2011, 2016)?

Our study will attempt to answer these questions using newly acquired wide-angle seismic (WAS) profiles (DIONYSUS, 2014, RV Meteor) oriented perpendicular to the Malta-Escarpment, which image the deep crustal structure of the eastern Sicily margin and adjacent Ionian basin (Calabrian accretionary wedge) (Figure 1).

2. Previous Work

2.1. Morpho-tectonic Structure of the Basin

Most of the morpho-tectonic structures of the Ionian basin (Figure 1) are related to the ongoing subduction and the development of its accretionary wedge. A thick (up to 10 km) low-taper accretionary wedge that is 200–300 km wide (in the downdip direction) has developed in front of the Calabrian and Peloritan blocks, which act as backstops. Today, this accretionary wedge can be divided into two different morpho-structural domains: a post-Messinian wedge to the south and south-east, consisting of a tectonically thickened evaporitic layer overlying undeformed Mesozoic and Cenozoic sediments, and a pre-Messinian wedge that does not contain Messinian evaporites (Gallais et al., 2012; Polonia et al., 2011).

Most of the Mediterranean basins were affected by the Messinian event that led to the deposition of a thick evaporite layer in the deeper areas of the basins. In the Ionian basin the accretionary wedge was first proposed to have developed above the base of the Messinian evaporite layer that act as a décollement (Finetti, 1982).Today, the growth of the accretionary wedge is proposed to have occurred in two stages defined by the Messinian evaporite deposits. The pre-Messinian wedge evolution may be explained by the Coulomb wedge model, whereas during post-Messinian times, the wedge growth was dominated by rapid forward propagation of the outer wedge above a décollement at the base of the Messinian evaporites, and possible underplating of the deeper Mesozoic to Cenozoic sediment layers (Gallais et al., 2012; Minelli & Faccenna, 2010). The wedge can also be divided laterally into two morphologically distinct lobes (Eastern and Western). The boundary between these lobes has been named the Ionian fault system (IFS) (Polonia et al., 2011).

2.2. Crustal Nature and Structure

The crustal structure of the Ionian basin was first explored during a WAS experiment using five ocean bottom seismometers (OBSs) and dynamite explosions (Makris et al., 1986). A NW-SE profile spanning the eastern Sicily margin indicated a crust of about 30 km thickness beneath the Sicilian-Hyblean platform that thins rapidly at the Malta Escarpment to a thin crust in the basin that is about 7 to 5 km thick to the east. The authors interpret the Malta Escarpment as a divergent continental margin formed during the Early Mesozoic and reactivated during the Miocene. Within the basin the thin crust was interpreted to be of oceanic origin.

The crust at the Ionian Abyssal Plain (IAP) was studied using Expanding Spread Profiles (de Voogd et al., 1992; Le Meur, 1997). Modeling results show a 5 km thick sedimentary cover overlying a crust of only 7 to 9 km thick. The depth of the Moho is observed at 16 to 18 km beneath the IAP, and the mantle layer is characterized by a high *P* wave velocity of 8.5 km/s. One study based on teleseismic *P* and *S* wave arrivals (D'Alessandro et al., 2016) and another based on multichannel seismic (MCS), potential field (gravity and magnetics), and geochemical data analysis (Polonia et al., 2017) have proposed the presence of a broad area of serpentinized mantle material beneath the Ionian Sea region, producing numerous serpentinite diapirs. These authors propose that the origin of this basement might be inherited from Mezosoic rifting and spreading fabric possibly reactivated by recent subduction processes.

A band of layered high-amplitude reflections near the base of the crust was imaged by seismic data in the western Ionian Sea and proposed to be related to volcanic activity in this region (Cernobori et al., 1996; Nicolich et al., 2000). The authors interpret the region as a passive margin and suggest the presence of oceanic crust in the basin. Moreover, this work also identified a major fault, now called the Alfeo fault system (AFS)

(Gutscher et al., 2016), east of the Malta Escarpment (Figure 1). This fault system clearly affects all sedimentary layers as well as the crust, likely reaching the upper mantle.

Based on the interpretation of MCS reflection lines, the Timpe faults, located on the eastern flank of Mount Etna in the southern prolongation of the Taormina line (Figure 1), are linked to steep active normal faults located offshore Catania and Augusta and affect the Malta Escarpment (Chiocci et al., 2011; Hirn et al., 1997; Palano, 2016). In later studies based on bathymetric mapping and high-resolution seismic reflection lines, the faults were observed to continue offshore (Gross et al., 2016) and possibly link to the major fault zone observed at the AFS (Gutscher et al., 2016). This major lithospheric scale fault is interpreted as the expression of a lateral slab tear fault (Gutscher et al., 2017).

Results from 3-D teleseismic tomography reveal the downgoing Calabrian slab as a structure extending 350 km laterally from northern Sicily to southern Campania and 400 km vertically (Amato et al., 1993; Cimini, 1999; Spakman et al., 1993). More refined mantle tomography revealed a 150 km wide slab window beneath the southern Apennines (Chiarabba et al., 2008; Piromallo & Morelli, 2003; Spakman & Wortel, 2004). The results suggest that the subducting lithosphere remains undetached only for a 100 km long segment along the central portion of the Calabrian arc (Chiarabba & Palano, 2017; Neri et al., 2009, 2012). The existence of a proposed STEP fault (Govers & Wortel, 2005; Wortel et al., 2009) was confirmed by tomographic and gravity modeling (Neri et al., 2012). Recent seismological and geodetic work provides evidence for toroidal flow around the retreating slab edges of the Calabrian subduction system (Baccheschi et al., 2011; Civello & Margheriti, 2004). This work identified clockwise rotations in Sicily and Calabrian and counterclockwise rotations in the southern Apennines that are predicted from the STEP model (Palano et al., 2017). Overall, a compilation of different tomography results suggests that the eastward migration of the slab edge follows the lithospheric transform fault of the Neo-Tethys ocean (Rosenbaum et al., 2008).

3. Objectives of the Study

3.1. Origin of the Ionian Basin

The first question evoked in this paper is the origin of the Ionian basin and its implication on the geodynamic processes. It is generally accepted that the Ionian basin was created during the Pangea breakup at the end of the Paleozoic or in the Early Mesozoic (Agard et al., 2011; Sage et al., 1997; Stampfli et al., 2002) when rifting formed the Tethys oceanic domain. Several branches formed during the opening of the Tethys Ocean; however, the timing of rifting, the exact number of branches, and the geometry of rifting remain controversial (Dercourt et al., 1986; Stampfli et al., 2002). Also debated is the question if the Western Alpine-Tethys and Eastern Neo-Tethys oceans were separated (Stampfli & Borel, 2004) or if they were connected near Sicily (Frizon de Lamotte et al., 2011; Jolivet et al., 2015). The Malta Escarpment is usually considered to be a remnant of the margin formed during the opening of the Ionian basin (Catalano et al., 2001; Frizon de Lamotte et al., 2011).

Several hypotheses exist for the opening processes forming the Ionian basin, but two prevail and will be discussed here. The first one proposes an E-W orthogonal opening, where the Malta-Escarpment and the Apulian Escarpment represent conjugate margins (Catalano et al., 2001). The second hypothesis proposes that a N-S opening occurred and that the Malta-Escarpment is a remnant of a transform margin (Frizon de Lamotte et al., 2011; Gallais et al., 2011). In this hypothesis the Ionian basin was a branch of the Neo-Tethys and represented a link between the Alpine-Tethys ocean (to the north-west of the Ionian basin) and the Neo-Tethys ocean (to the east).

3.2. Nature of the Crust

Concerning the nature of the crust in the Ionian basin, we test two main hypotheses. The first hypothesis suggests that the crust at the bottom of the basin is thinned continental crust, originating from a distal portion of the North African continental margin (Roure et al., 2012). Several arguments are in favor of this hypothesis, such as the absence of a clearly visible oceanic spreading center, and the strong similarities in structural styles and timing of inversion between the Saharan Atlas, Sicilian Channel, and the IAP that might imply that all three regions belong to the continental margin of north-African domain. An additional argument is the fact that no lithospheric-scale faults are observed offsetting the Moho in the Apulia/Adriatic and the eastern and central Mediterranean domains, implying that these belong to a distal thinned continental portion of the

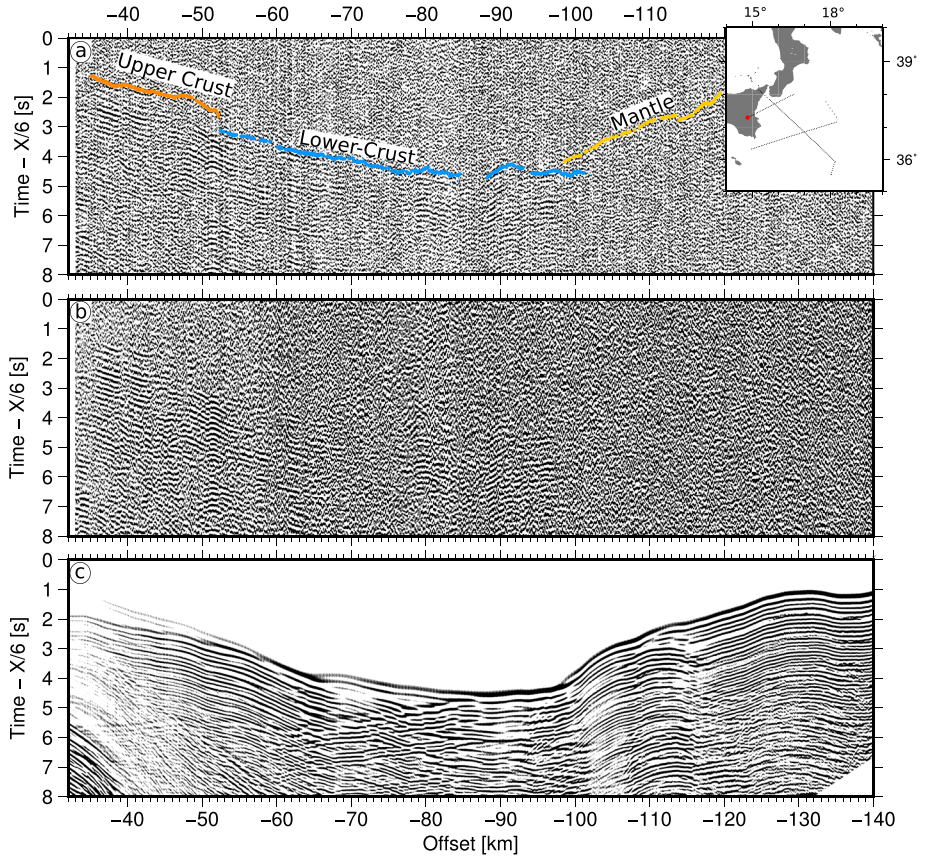

Figure 2. Example of the data acquired by the land station 6 of the northern DYP3 profile. (a) Interpretation of the seismic section preprocessed with annotation of each phases identified: upper crust, lower crust, and Mantle refraction phases. (b) Raw seismic section of the land station 6. (c) Synthetic arrivals calculated from the velocity model with location map of the station.

North-African plate (Roure et al., 2012, and references therein). Other authors also evoke the structural continuity of the Medina seamounts that are proven to be of a continental affinity (Finetti, 1982).

The second hypothesis proposes that the nature of the crust of the Ionian basin is oceanic. The arguments raised by these authors are based on the interpretation of various sets of geophysical data and modeling of reflection and WAS data (Catalano et al., 2001; Cernobori et al., 1996; de Voogd et al., 1992; Gallais et al., 2011; Le Meur, 1997; Makris et al., 1986; Nicolich et al., 2000; Speranza et al., 2012). Several studies observed a thin crust with velocity gradients that are in good agreement with those of typical oceanic crust (White et al., 1992). However, the exact number of layers in the crust (2 or 3) remains controversial. In these studies the very low heat-flux values (30–40 mW/m^2) (Della Vedova et al., 1989) observed in the central and eastern portions of the basin are interpreted as linked to the oceanic origin. The old age of the lithosphere and the high Bouguer gravity anomaly suggest a shallow Moho discontinuity.

3.3. STEP Fault Location

The roll-back of a broad NW dipping subduction beneath the SW European margin (current-day SE France and E Spain) provoked the detachment of the AlKaPeCa continental terranes from the European plate and their migration toward the south and south-east during the last 35 Ma (Lallemand & Funiciello, 2009; Rehault et al., 1984; Ricou, 1994). Since the late Miocene (8 Ma), the roll-back movement reached the Ionian basin with its particular situation of being a narrow oceanic domain located between two continental ones (Africa with Sicily to the west and SW and Apulia to the N-E). Because of the particular tectonic setting, one or more slab segmentation and major lithospheric faults have been proposed to accommodate the subduction of the very narrow oceanic domain and the slab roll-back. This mechanism is considered to represent

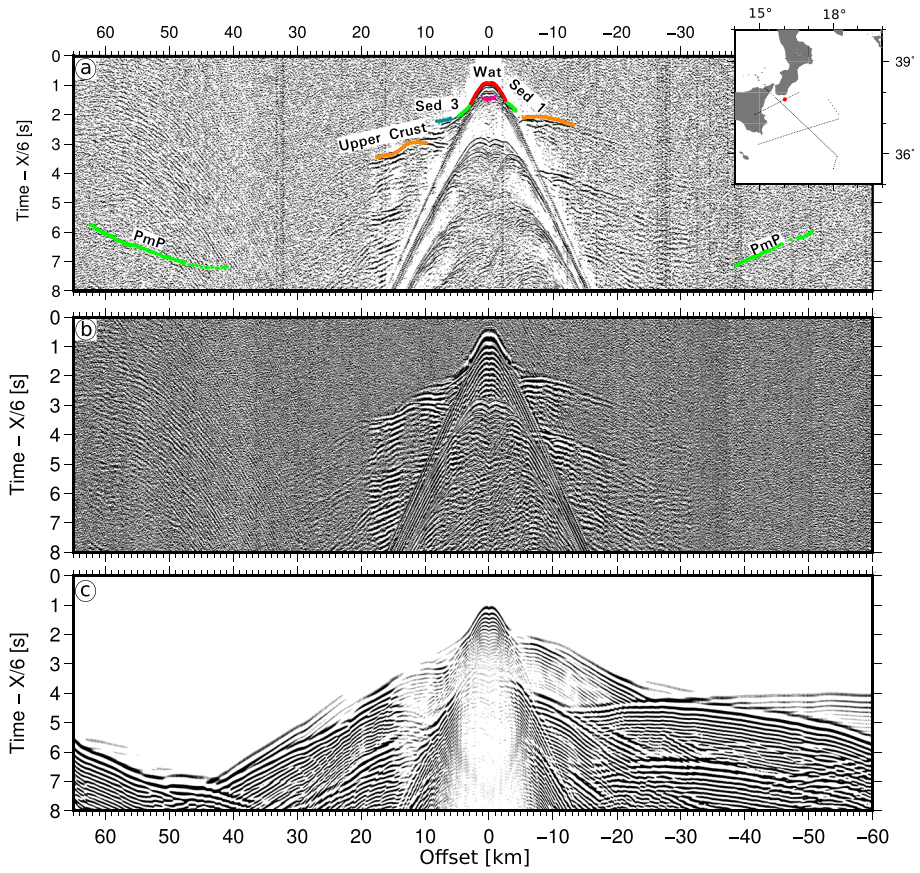

Figure 3. Seismic section of the ocean bottom seismometer (OBS) 10 on DYP3 profile. (a) Interpretation of the seismic section preprocessed with annotation of each phases identified: Wat (for Water direct arrival), Sed 1 (for Shallow sediments), sed 2 (for deeper sediments), and upper-crustal refraction phases. (b) Raw seismic section of OBS 20. (c) Synthetic arrivals calculated from the velocity model. And a location map of the OBS observed.

a STEP fault accommodating the roll-back of the subduction along its edge (Gallais et al., 2013; Govers & Wortel, 2005; Rosenbaum et al., 2008). Although most authors agree on the existence of such a STEP fault in the western part of the basin, its exact location remains the object of debate.

Today three hypotheses exist for the location of the STEP fault. According to the first one, the STEP fault is situated at the foot of the Malta Escarpment, mainly because the escarpment represents the dominant morphological structure of the basin. Also, several recently active fault-oriented NNW-SSE and an uplift of a 20–30 km wide region were observed at the foot and east of the Malta Escarpment in seismic reflection profiles (Argnani & Bonazzi, 2005).

The second hypothesis considers the IFS as the STEP fault location. The IFS is described as a major crustal-scale fault zone between the two lobes (Eastern and Western) of the accretionary wedge. It was identified from seismic reflection profiles and complementary morpho-bathymetric studies (Polonia et al., 2011, 2016).

The third hypothesis also based on swath bathymetric and seismic reflection observations places the STEP fault along the AFS (Gallais et al., 2013; Gutscher et al., 2016, 2017). The AFS trends in a roughly N-S direction, about 40 km east of the Malta Escarpment and parallel to it, and veers to N-W reaching Mount Etna to the north (Gallais et al., 2012; Gutscher et al., 2016, 2017). According to deep seismic investigations the faults affect the crust and may reach the upper mantle (Nicolich et al., 2000). Moreover, this hypothesis is supported by the location of Etna volcano relative to the arc of the subduction (Eolian islands), as well as the geochemistry of its expelled volcanic rocks showing a mantle origin (Schiano et al., 2001). In this context it is important to keep in mind that the propositions of the location of the fault were made based on surface and shallow subsurface data (reflection seismic and swath bathymetry data). They image a deformation zone

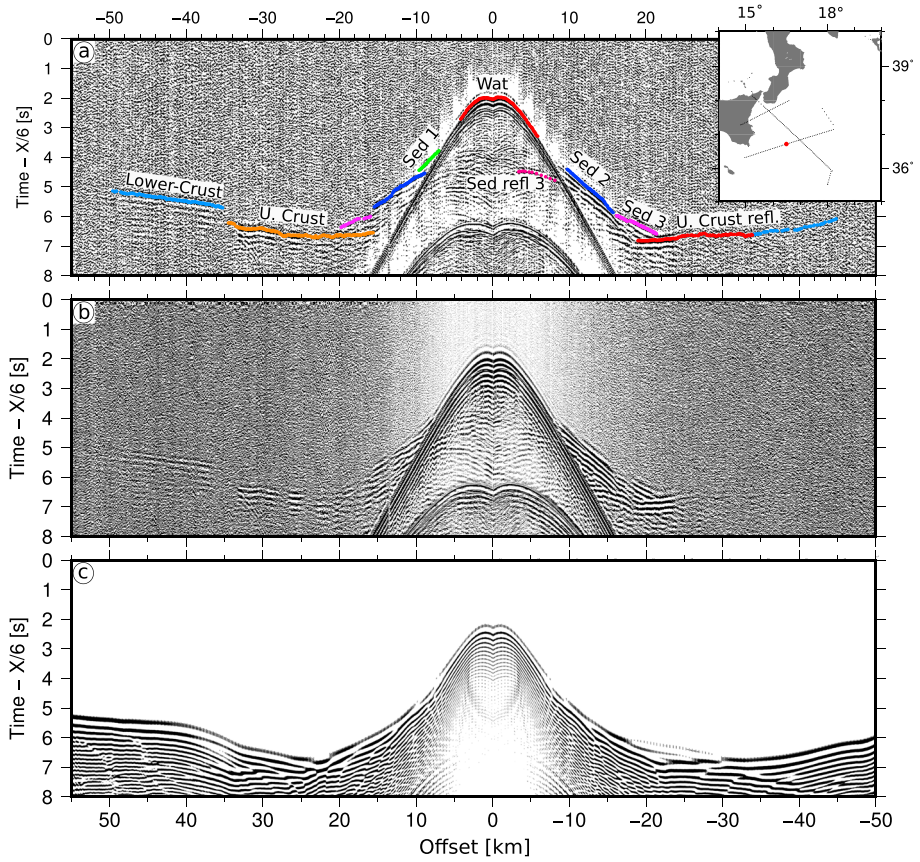

Figure 4. Seismic section of the ocean bottom seismometer (OBS) 25 on DYP1 profile. (a) Interpretation of the seismic section preprocessed with annotation of each phases identified: Wat (for Water direct arrival), Sed 1 (for Shallow sediments), sed 2 (for deeper sediments), sed 3 (for deeper sediments), U. Crust (for Upper-crust), and Lower Crust refraction phases. And sed refl 3 (for sedimentary reflection phase) and U. Crust Refl. (for upper-crustal reflections). (b) Raw seismic section of OBS 25. (c) Synthetic arrivals calculated from the velocity model. And a location map of the OBS observed.

by combination of normal and strike-slip faults that might correspond to a deep lithospheric STEP fault, which itself cannot be imaged by these data.

4. Wide-Angle Seismic Data Acquisition

In order to answer the questions regarding the deep structure and the nature of the crust in the Ionian basin, we acquired regional WAS (Figures 2–5) and MCS data during the DIONYSUS experiment together with bathymetric swathmapping data.

4.1. The DIONYSUS Project

This DIONYSUS project was a collaboration of four institutes: the University of Western Brittany (Brest, France), Geomar (Kiel, Germany), Ifremer (Brest, France), and Istituto Nazionale di Geofisica e Vulcanologia (INGV) (Rome, Italy). The survey took place in October 2014 aboard the R/V Meteor, cruise M111. Five profiles were acquired during the survey: two of them are perpendicular to the eastern Sicily margin (DYP1 and DYP3), one in the IAP (DYP5), a line crossing these three in a NW-SE direction (DYP4), and a short line (DYP2) on the Eastern lobe of the accretionary wedge (Figure 1). This work will focus on the two margin-perpendicular profiles, DYP3 in the north and DYP1 in the south.

The instruments deployed on the northern DYP3 profile were 12 OBSs from Ifremer (Auffret et al., 2004) and 13 OBHs (ocean bottom hydrophones) from Geomar (Bialas & Flueh, 1999), for a total of 25 OBS/H and six land stations from the INGV of Rome. Along profile DYP1, we deployed 26 OBS from Ifremer and 26 OBH from Geomar for a total of 52 instruments. Along both profiles the instrument spacing was 6 km. The OBS used in the experiment were 32 MicrOBS (+) from Sercel (Auffret et al., 2004) that include three-component

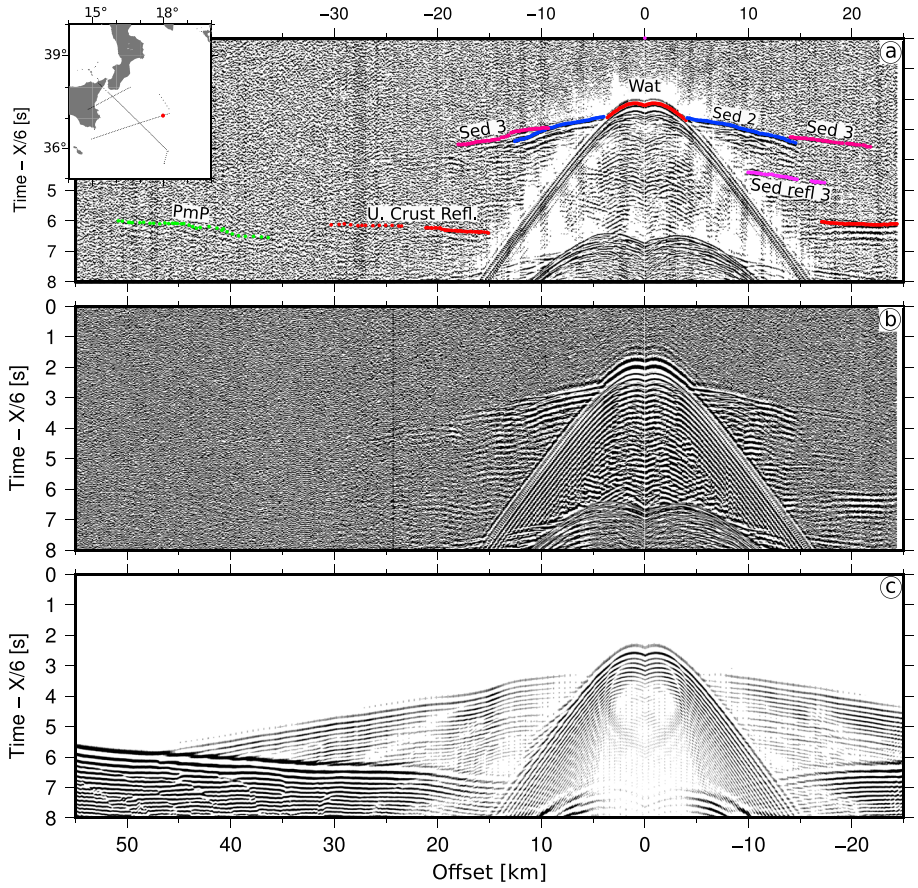

Figure 5. Seismic section of the ocean bottom seismometer (OBS) 48 on DYP1 profile. (a) Interpretation of the seismic section preprocessed with annotation of each phases identified: Wat (for Water reflection arrival), sed 2 (for sediments), sed 3 (for deeper sediments), U. Crust Refl. (for upper-crustal reflections), and PmP (for Moho reflection phase). (b) Raw seismic section of OBS 48. (c) Synthetic arrivals calculated from the velocity model. And location map of the OBS.

geophones that can record frequencies from 4.5 Hz to 1 kHz and one hydrophone that record from 4 Hz to 15 kHz at the same sampling rate. The OBH records only with a hydrophone (HTI-01-PCA hydrophone from HIGH TECH INC) (Bialas & Flueh, 1999). The land stations on profile DYP3 were six REF TEK 130S-01 equipped with velocimeter sensors of short-period Lennartz LE-3Dlite with a 1 s dominant period. The sampling rate of the stations was set at 8 ms (Moretti et al., 2015).

The seismic source used during the survey consisted of two subarrays of six GI-Guns from Sercel Marine Sources Division and Seismograph Services Incorporation. The 12 GI-Guns were operated simultaneously; they provided a volume of 84 L (5,440 in^3) at ~190 bar. The shooting interval was set at 60 s for all profiles, resulting in a shot point distance of 150 m at 5 knots.

4.2. Data Quality and Initial Processing

Two OBSs (7 and 16 of line DYP3) were lost during the cruise, but all other instruments provided relatively good quality data on both the geophone and hydrophone channels. Arrivals are locally strongly attenuated due to an irregular salt layer in the Ionian basin. Also, the seismic energy is lost at offsets exceeding 40 km on the OBS data on some instruments, probably due to the presence of strongly reworked sediments and/or poor coupling (Figures 3–5). The land stations recorded arrivals up to larger offsets than the OBS (120 km), thus allowing us to additionally constrain the deep geometry of the crust and the Moho discontinuity (Figure 2).

On the southern profile DYP1, the data of two OBS are missing (17 and 33 on line DYP1) due to malfunctioning of the instruments; however, the data quality on the rest of the profile is better than for the northern

Table 1
Summary Table of the Main Uncertainties for the DYP3 and DYP1 Velocity Models for Each Phases

DYP3 profile	Phase number	Picking error (ms)	Layer code	Number of picks	Error RMS	Error χ^2
Water	1	0.03	1.2	1,288	0.019	0.386
Sediments 1	2	0.07	3.1	825	0.093	1.758
Sediments 2	3	0.07	4.1	191	0.053	0.566
Sediments 1 reflection	4	0.08	2.2	264	0.145	3.314
Sediments 2 reflection	5	0.08	3.2	175	0.087	1.195
Basement	6	0.1	6.1	1,605	0.134	1.792
PmP	7	0.12	7.2	465	0.159	1.749
Pn	8	0.13	8.1	134	0.18	1.935
Sediments 3	9	0.08	5.1	221	0.09	1.266
Lower crust	11	0.1	7.1	648	0.124	1.542
Lower-crust reflection	12	0.1	6.2	40	0.275	7.734
Basement reflection	17	0.1	5.2	54	0.068	0.474
DYP1 profile						
Water	1	0.030	1.2	3,171	0.029	0.942
Sediments 1	2	0.070	2.1	1,066	0.115	2.693
Sediments 2	3	0.070	3.1	4,277	0.096	1.900
Sediments 1 reflection	4	0.080	2.2	421	0.093	1.350
Sediments 2 reflection	5	0.080	3.2	1,455	0.103	1.648
Basement	6	0.100	6.1	3,242	0.128	1.631
PmP	7	0.120	7.2	891	0.206	2.945
Pn	8	0.130	8.1	473	0.206	2.526
Sediments 3 reflection	10	0.080	4.2	1,227	0.092	1.332
Lower crust	11	0.100	5.1	2,501	0.127	1.616
Basement reflection	17	0.100	5.2	787	0.154	2.368

Note. The "basement" is the upper crust, "PmP" is the reflection on the Moho discontinuity, and "Pn" is the refracted phase in the mantle layer.

profile. The interpretation of the data from the OBS on the westernmost part of the profile (OBS 1 to 11) was difficult because of the shallow water depth (100 m) that led to strong reverberations in the seismic section. The OBS between 32 and 41 recorded a highly attenuated signal, probably because of the reworked sediments and the thick Messinian evaporitic layer (Figures 4 and 5).

All of the stations were relocated using the direct arrival of the seismic shots, thus providing an exact position for each OBS along both profiles. The interpretation of the OBS data was done following the example shown in Figures 2–5. The data were picked on unfiltered record sections for the closest shots and using a band-pass filter, a deconvolution, an automatic gain control, and spectral whitening for the larger offsets. A picking uncertainty was assigned to each phase, based on the data quality and offset, and is presented in Table 1 for both profiles and all phases.

4.3. Forward Modeling

The data were modeled using the two-dimensional forward modeling module of the RAYINVR software (Zelt & Smith, 1992). The code performs a combined forward ray-tracing and damped inversion modeling of WAS data. The models are defined by layers defined at regular or irregular node-spacing and have associated velocities that can vary laterally. All parameters can be inversed either separately or together (for details on the calculation, model parameterization, and modeling strategy see Zelt, 1999). The modeling process is performed by calculating theoretical arrivals from a two-dimensional starting velocity model that is manually adjusted to fit the picked OBS data *P* wave traveltimes, layer by layer and from the top to the bottom of the model. The quality of the fit is given by the RMS (root-mean-square) traveltime residual and χ^2 error for all phases of each arrival (Table 1). The seafloor layer is constrained by the bathymetric data acquired during the cruise. The velocity model is extended by 30 km on both ends and 10 km deeper than the zone covered by seismic rays to avoid side effects. For velocity nodes, an iterative damped least squares traveltime inversion, from the RAYINVR software, was additionally used to improve data fitting.

For the model parameterization, a minimum structure/parameter approach was used to avoid inclusion of structures (or velocities) unconstrained by the data. Minimal lateral velocity changes were added, and only

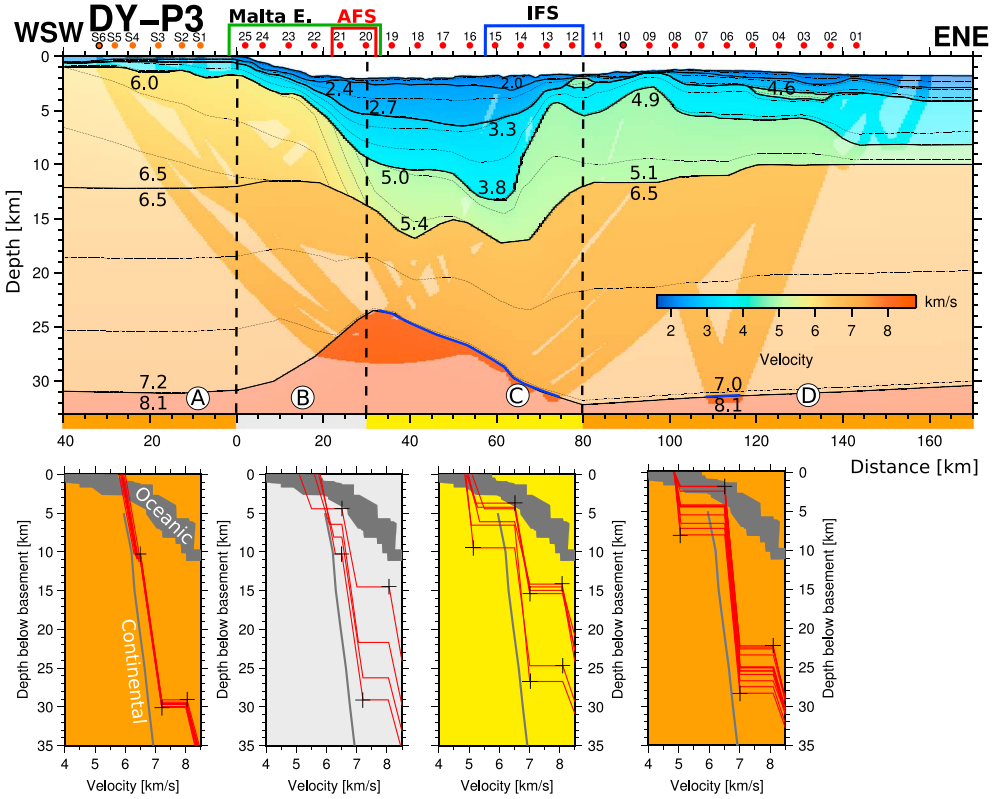

Figure 6. Northern DYP3 velocity model obtained by forward modeling of the ocean bottom seismometer (the red dots show their location along the profile) and land stations (oranges dots) data. The strongly shaded areas show where the model is constrained by seismic rays, while the pale ones are constrained by our gravimetric analysis. The black numbers are the velocities in km/s. The thick line are the limits of the model's layers, while the thin line are the iso-velocity lines set every 0.25 km/s. The blue lines show the Moho reflections picked from the ocean bottom seismometer data. The model is cut into four domains according to their general structures, see text for detailed description. Below, are presented the velocity-depth profiles, extracted from the velocity models every 10 km and underneath the top of the upper-crust (that is at 0 km of depth). The black crosses represent the error bar extracted from the Monte Carlo analysis (Figure S2 of the supporting information). The areas in dark gray represent the range of typical velocity-depth profiles observed for oceanic and continental crust (Christensen & Mooney, 1995; White et al., 1992). The colors correspond to our interpretation from these results: orange for continental, gray for thinning/transition, yellow for thinned continental, and violet for oceanic domains. The zone of influence of the structures are presented in green, red, and blue rectangles that are respectively the Malta-Escarpment, the Alfeo fault system, and the Ionian Fault system.

when required by the data. Each layer was added based on a reflection arrival in the data or because velocity gradients were needed to explain all of the arrivals on several different OBS data. Also, the three upper sedimentary layers were picked and extracted from the coincident reflection seismic data acquired during the cruise that were converted into depth using velocities from the velocity model. A depth-converted section of the previously published CROP3 profile (Polonia et al., 2011), coincident with the WAS DYP1, was also used to define the upper sedimentary layers. The deeper layers were modeled only from the OBS data, and for the Moho depth additional constraints were taken from the literature (de Voogd et al., 1992; Makris et al., 1986; Nicolich et al., 2000) and our gravity analysis. Velocity gradients and phase identification from the velocity model were also constrained by a synthetic seismogram analysis using the finite difference modeling code from the Seismic Unix Package (Stockwell, 1999; Stockwell & Cohen, 2003) (Figures 2c to 5c).

5. Results

5.1. Velocity Models

5.1.1. Northern DYP3 Velocity Model

The northern DYP3 profile includes eight layers: the water column, four sedimentary layers, two crustal, and the mantle layer (Figure 6). The seafloor was extracted from a high-resolution swath bathymetric map (Gutscher

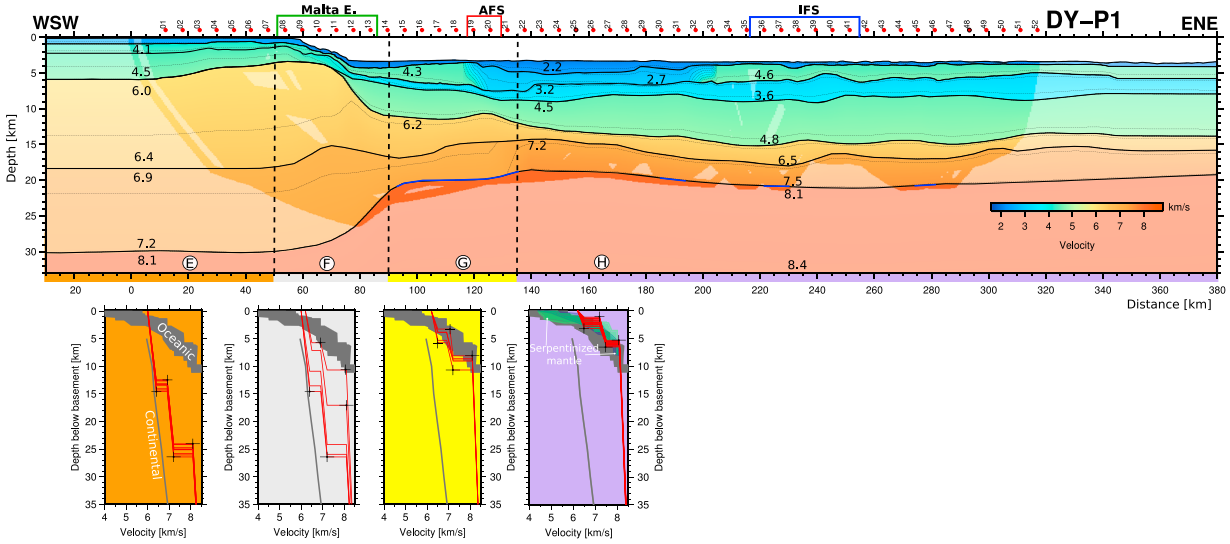

Figure 7. Southern DYP1 velocity model, obtained by forward modeling of the ocean bottom seismometer (OBS) data (the red dots show their location along the profile, and the black circles are the OBS shown). The strongly shaded areas show where the model is constrained by seismic rays, while the pale ones are constrained by our gravimetric analysis. The black numbers are the velocities in km/s. The thick lines are the limits of the model's layers, while the thin line are the iso-velocity lines set every 0.25 km/s. The blue lines show the Moho reflections picked from the OBS data. The model is cut into four domains according to their general structures, see text for detailed description. Below are presented the velocity-depth profiles, extracted from the velocity models every 10 km and underneath the top of the upper-crust (that is at 0 km of depth). The black crosses represent the error bar extracted from the Monte Carlo analysis (Figure S2 of the supporting information). The areas in dark gray represent the range of typical velocity-depth profiles observed for oceanic (White et al., 1992) and continental crust (Christensen & Mooney, 1995), green for serpentinized mantle (Dean et al., 2000), and blue from deep Tyrrhenian sea basins (Prada et al., 2015). The colors correspond to our interpretation from these results: orange for continental, gray for thinning/transition, yellow for thinned continental, and violet for oceanic domains. The zone of influence of the structures are presented in green, red, and blue rectangles that are respectively the Malta-Escarpment, the Alfeo fault system, and the Ionian Fault system.

et al., 2017). The water velocity was set to 1.53 km/s from the first reflection arrivals in the OBS data and is in good agreement with other WAS studies in the Mediterranean Sea (e.g., Leprêtre et al., 2013). The model can be subdivided into four domains, called A, B, C, and D (Figure 6). Domains A and B correspond to the Sicilian block with unthinned and thinned crust. Domain C comprises the basin and D the Calabrian Block.

Along domain A three sedimentary layers were modeled, with a variable thickness of 1–3 km, thickening toward the east. The crust comprises two distinct layers of a combined thickness around 30 km. Velocities vary between 6.00 km/s at the top and 7.20 km/s at the base. In domain B the sedimentary layers thicken from 3 to 9 km along the slope. The crustal thickness decreases to 15 km, and the velocities of the upper crustal layer decrease toward the east from 6.00 to 5.00 km/s in 15 km of lateral distance. The sedimentary thickness is highest in domain C reaching up to 12 km at the position of OBS 15. The crustal layers are deepening toward the east by about 5 km and at 70 km model distance. From that position the crustal layer thickness increases abruptly, limiting the sedimentary basin in an asymmetrical way. In domain D the sedimentary layers are of variable thicknesses, between 3 and 7 km increasing toward the ENE. Only in this domain a fourth sedimentary layer characterized by velocities around 4.6 km/s, higher than those of the underlying layer, can be observed. The crustal layers are around 25 km thick and thus thinner than in domain A, and the velocities span from 4.90 to 7.00 km/s. The upper mantle velocities were set to 8.00 km/s at the top and 8.40 km/s at the base of the layer along the complete model, based mainly on arrivals from the basin, but also from the literature (de Voogd et al., 1992; Makris et al., 1986; Nicolich et al., 2000) and from our gravity analysis (Figures 6 and 8).

5.1.2. Southern DYP1 Velocity Model

The southern DYP1 profile comprises the same number of layers and can be subdivided into four different domains (E–H; see Figure 7). The E and F domains represent two parts of the Sicilian-Hyblean plateau with domain E representing its unthinned part and domain F corresponding to the Malta Escarpment. The remaining domains G and H are located in the basin, with domain G located at the foot of the escarpment and characterized by a slightly thicker crust than the rest of the basin, which forms domain H. Both domains are separated by the AFS.

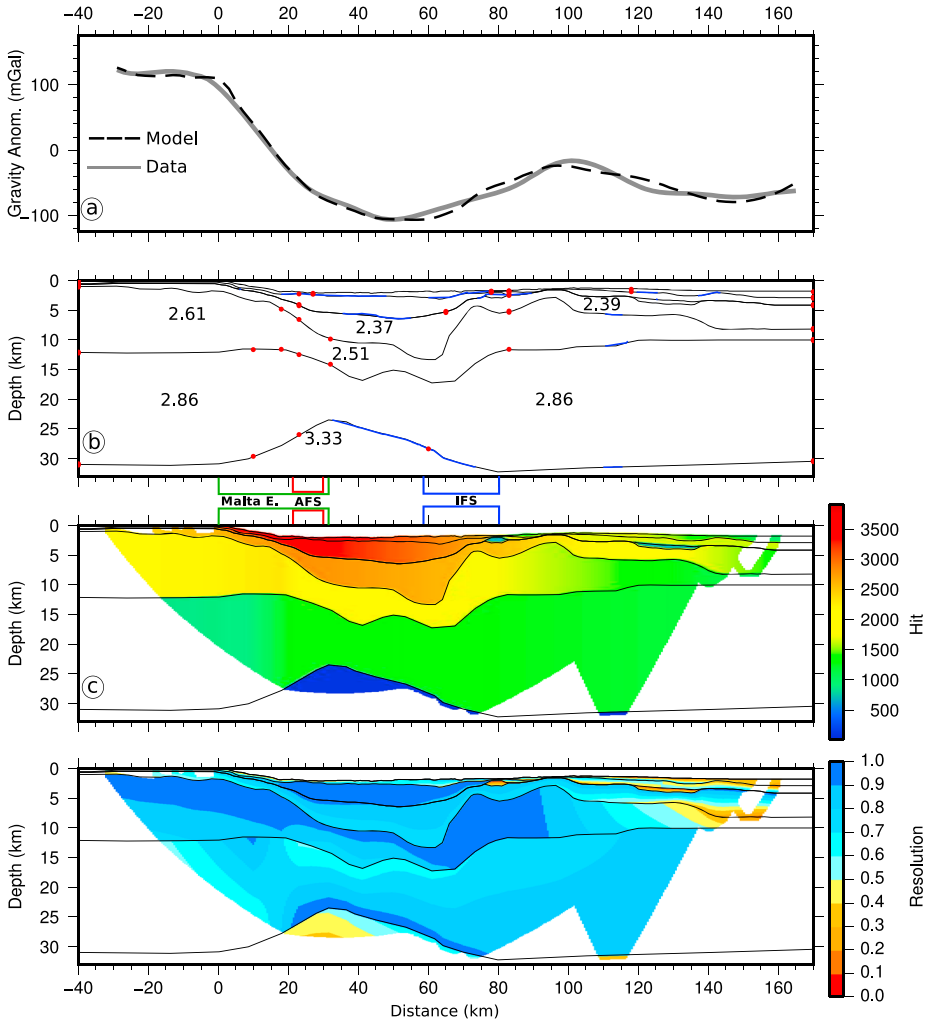

Figure 8. DYP3 velocity model evaluation. (a) Gravity model extracted from the velocity model (dashed black line) compare to data from satellite altimetry (solid gray). (b) Observed reflections from ocean bottom seismometer data, model layer limits (solid black lines), top and bottom velocity/depth nodes (red points), and reflection arrivals picked from ocean bottom seismometer data (blue interfaces). The black numbers are densities used for the gravity modeling. (c) Hit-count for velocity (gridded and colored). (d) Resolution of velocity (gridded and colored). Zones that were not images are blanked.

Sedimentary thickness in domain E is around 5 km, and three separate layers have been modeled. The velocities of these layers increase from 2.40 to 2.60 km/s for the first layer and from 4.35 to 4.65 km/s for the deepest sedimentary layer. Along domain E crustal arrivals are modeled with two layers that are 15 km thick for the upper crust with velocities between 6.00 and 6.40 km/s and 11 km thick for the lower crust with velocities of 6.91 to 7.21 km/s. Sedimentary layer thickness at the Malta escarpment (domain F) is around 2–3 km, lower than in domain E. However, one additional layer was identified and characterized by velocities between 4.50 and 4.80 km/s and a thickness of 2–3 km. The sedimentary layer thickness increases to up to 7 km eastward in this domain. The two crustal layers here show rapid thinning from a combined thickness of 25 km to 10–12 km at the foot of the escarpment at a lateral distance of only 40 km. Along domain G the sedimentary layer thickness increases to up to 8–10 km. Here a velocity inversion has been modeled between the second layer, characterized by velocities between 4.30 and 4.60 km/s and the third layer with velocities between 3.20 and 3.60 km/s. This domain has been modeled by two distinct crustal layers having velocities between 6.20 and 7.00 km/s and a thickness of 8–10 km and a similar layer thickness of 4–5 km. The neighboring domain H represents the deep basin with a sedimentary infill between 8 and 12 km thick, here separated into four layers. A velocity inversion similar to that of domain G is modeled east of OBS 33. The highest sedimentary

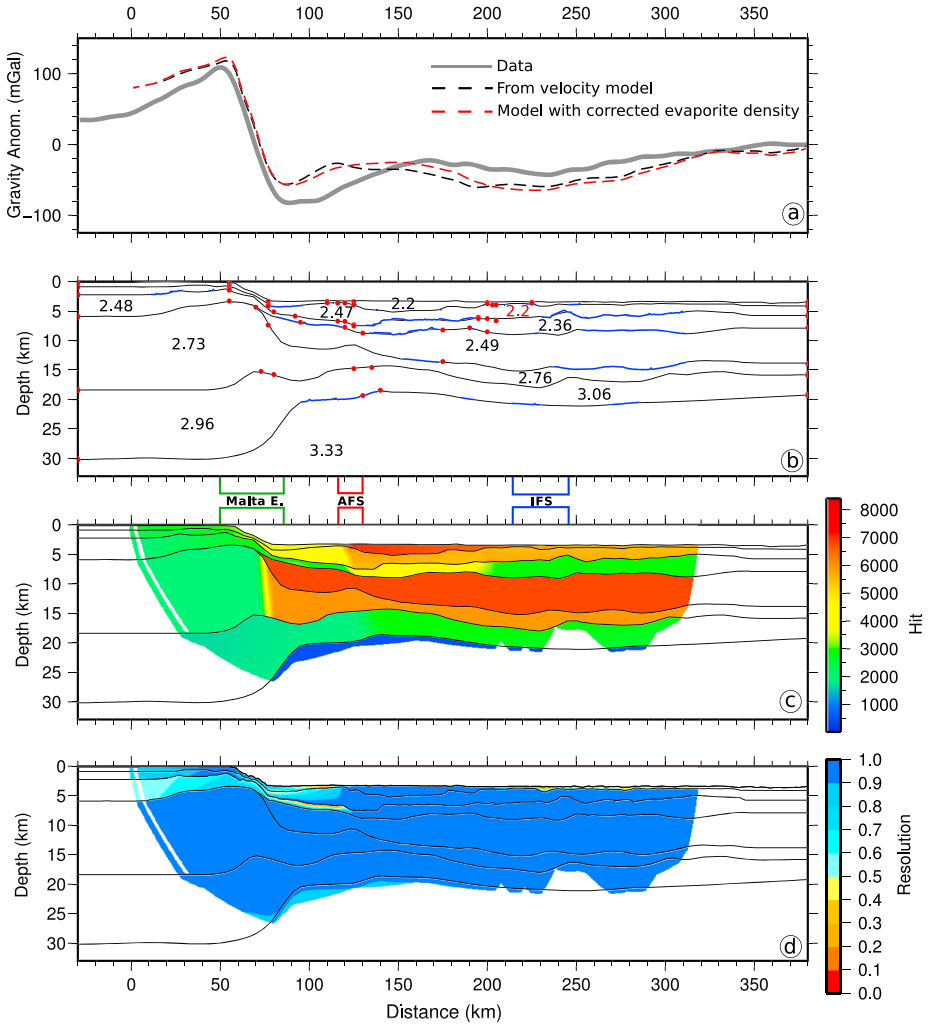

Figure 9. DYP1 velocity model evaluation. (a) Gravity model extracted from the velocity model with the direct velocity density correlation (dashed black line) and corrected evaporite density applied to the high-velocity layer (dashed red line) compared to data from satellite altimetry (solid gray). (b) Observed reflections from ocean bottom seismometer data, model layer limits (solid black lines), top and bottom velocity/depth nodes (red points), and reflection arrivals picked from ocean bottom seismometer data (blue interfaces). The black numbers are densities used for the gravity modeling, and the red one is the corrected density. (c) Hit-count for velocity (gridded and colored). (d) Resolution of velocity (gridded and colored). Zones that were not imaged are white.

velocities of 4.8 km/s have been modeled in the center of the basin. Although the crust modeled in this domain H is similar to that of domain G, but two main differences have been modeled. The crust is 1–2 km thinner, and the upper layer is distinctly thinner than the lower layer. Lower crustal velocities are slightly higher reaching up to 7.3 km/s.

All mantle layer velocities were set to be constant between 8.10 km/s at the Moho interface and 8.40 km/s at the bottom of the model. Those velocities were chosen according to upper mantle arrivals (Pn) from 18 instruments recordings between the OBS 08 and the 51.

5.2. Error Analysis

The resolution parameter is based on the number of rays passing a single-velocity node (Figures 8d and 9d). It is therefore dependent on the number of velocity nodes in each layer and can be used to avoid overparameterization of the model (Zelt, 1999). If a layer is constrained by one single-velocity node, the resolution parameter will be 1. Nodes showing a resolution value greater than 0.5 are considered to be well constrained, and a layer showing an overall resolution over 0.5 is considered as not overparameterized. Where the model is

constrained by reflection phases, the depth of each layer is well constrained (blue lines in Figures 8b and 9b). The ray density provides the number of rays in each cell of the velocity model. Regions with high ray coverage are well constrained (Figures 8c and 9c).

The synthetic seismogram analysis (Figures 2c to 5c) allows us to constrain the velocity gradients of all layers. The finite difference modeling code from the Seismic Unix package (Cohen & Stockwell, 2003; Stockwell, 1999) was used to calculate synthetic seismograms. The input velocity model was calculated from sampling the forward velocity model at a lateral 25 m interval and 10 m interval in depth. Overall, along both profiles, the synthetic seismograms reproduce well the amplitudes and arrival times of the OBS data, showing that the velocity models take into account the majority of the observed phases.

5.2.1. On the DYP3 Profile

The quality of the model is given by the difference between the modeled traveltimes and those picked in the data. The DYP3 model explains 5,910 picks out of 7,367 picks identified from the data, and their uncertainties are given in Table 1. The final RMS traveltime residual, between the model and the data, is 0.112 ms, and the resulting normalized chi-square is 1.469. The northern velocity model is well constrained along most of the profile except for the deeper layers and the ends of the model. The data quality allowed picking of only relatively few reflected arrivals from the OBS data, and they originate mostly from the three uppermost sedimentary layers and the Moho interface due to the higher impedance increase along these interfaces (Figure 8b). From the hit-count and resolution figures (Figure 8d), it can be observed that the less constrained areas are located in the deeper part of the model. The lower crust and the mantle layers show low hit-count values (Figure 8c). These results can be explained by a lack of late arrivals on the OBS sections for these domains, due to a low quality of the data at offsets greater than 40 km. Concerning the upper parts, the model is more robust due to a better ray coverage, as is attested by high hit-count values and resolution values exceeding 0.5.

5.2.2. On the DYP1 Profile

The DYP1 model uses 19,511 picks out of 23,160 picks identified from the data, and their uncertainties are summarized in Table 1. The final RMS traveltime residual, between the model and the data, is 0.114 ms, and the resulting normalized chi-square is 1.721. The resolution of the southern velocity model is very good along the entire profile, meaning that the velocity/depth nodes used to define the model are justified and are covered by a high number of seismic rays (Figure 9). The reflections from the OBS data are well distributed along the profile for the sedimentary layers and the Moho interface. Due to the fact that the overlying layer is a high-velocity layer, the third sedimentary layer is constrained by refracted phases only. The fourth sedimentary layer is mostly constrained by reflected phases and few refracted phases, implying that its internal velocities are only partially constrained by the OBS data. This is due to the fact that the overlying layer has a higher velocity. The velocity gradients used for this layer are adapted from Makris et al. (1986), who used deep seismic sounding along a profile crossing the Malta Escarpment (oriented WNW-ESE); Catalano et al. (2001), who studied the CROP-M3 profile coincident to our DYP1 profile; and from Gallais et al. (2011), who examined Expanding Spread Profiles data further south of the profile in the IAP. Also, the later arrivals in the OBS data were used to constrain these velocities (Figure 9). The hit-count values (Figure 9c) gradually decrease toward the base of the profile as expected; thus, the lower crust and mantle layers have the lowest hit-count values because of fewer rays reaching the base. The third sedimentary layer is characterized by a low number of rays due to the high-velocity overlying layer preventing turning rays in this layer. Laterally, the Malta Escarpment shows lower hit-count values than the rest of the profile due to the fewer instruments located on the escarpment. The mantle layer is mainly constrained by seismic rays between OBS 08 and 51 along the profile, and the velocities of 8.10 to 8.40 km/s were used to model turning rays from the upper mantle. Also, the depth of the Moho discontinuity is extrapolated from these observations, our gravity analysis, and the literature (de Voogd et al., 1992; Makris et al., 1986; Nicolich et al., 2000). A detailed uncertainty calculation including a perturbation (Figure S1 of supporting information) and a Monte Carlo (Figure S2, using Loureiro et al., 2016 software) analysis is presented in the supporting information. The ray coverage for sedimentary, crustal, and Moho interfaces are also presented in Figures S3 and S4.

5.3. Gravity Modeling

The velocity model can be additionally constrained by gravity modeling. For this the relationship between seismic velocity and density can be used to calculate an expected gravity anomaly from the ensuing

density model. The *Gravmod* software of Colin Zelt calculates trapezoids of constant density along each model layer from the velocity modeling associating a mean density from its velocity to each trapezoid using an empirical velocity-density relationship (Ludwig et al., 1970). This calculated anomaly can be compared to the free-air gravity anomaly obtained from satellite altimetry (Sandwell & Smith, 1997). This technique can help to constrain the portions of the model that are not penetrated by WAS data. As the deeper mantle layer, which is not constrained by the velocity model, can affect the results of this method, this layer is set to 3.32 g/cm^3 density along the whole profile on both models. Also, to avoid edge effects, all layers are extended by 30 km on both sides and have a maximum depth of 90 km.

5.3.1. Results for the DYP3 Gravity Profile

The results obtained for the northern DYP3 velocity model show a good fit between the free-air anomaly extracted from our density model and the gravity anomaly obtained by satellite altimetry (Bonvalot et al., 2012; Figures 8a and 8b). The gravity model provides better constraints on the deeper parts of the velocity model, especially for the eastern part of the model that is not well covered by seismic rays. Here the results obtained by the gravity anomaly modeling are good and provide new constraints on the deeper part of the velocity model (Figures 8a and 8b). The mantle layer was adjusted to fit the data at 30 km of model offset by a lower density of 3.30 g/cm^3 in agreement with the fact that it is a geological transition zone.

5.3.2. Results for the DYP1 Gravity Profile

On the southern profile (Figures 9a and 9b), the fit between the gravity anomaly extracted from the model and the observed anomaly is less satisfactory using the empirical velocity-density relationship only than along the northern profile. However, the large-scale features are well explained by our velocity model. In detail, the fit is moderate between 75 and 120 km of offset along the profile and the discrepancy results from an excess of mass in our model. One explanation is that the method relies on the direct conversion of velocities into density. In the velocity model, this region corresponds to the thickest part of the shallow high-velocity layer that is interpreted by numerous studies to represent the Messinian evaporites (Gallais et al., 2011; Gailler et al., 2009; Leprêtre et al., 2013; Nicolich et al., 2000; Polonia et al., 2016). However, evaporites have high seismic velocities due to their crystalline structure, but low densities (de Voogd et al., 1992; Trippetta et al., 2010), so the direct conversion can then not be applied to this specific layer. The gravity anomaly was modeled again using a value of typical evaporite density (red value in Figure 9b), and the results obtained provide a better fit where the evaporite layer is the thickest along the profile (Figure 9a). The remaining misfit cannot be explained by the presence of evaporites along the model and probably is due either to regional density variations in the mantle, which cannot be explained by our velocity model, or alternatively may be caused by three-dimensional variations of the Moho topography.

6. Discussion

In the sections below, we discuss the implications of our results for the opening of the basin, the crustal nature, and the location of the STEP fault.

6.1. Interpretation of DYP3 Profile

The DYP3 profile is located in a region where ancient structures (e.g., the Malta escarpment), formed by the opening of the Tethys, are interacting with more recent structures, originating from the active subduction and slab roll-back. This creates a complicated, highly three-dimensional configuration. Along the northern DYP3 profile, the upper sedimentary layer velocities do not vary significantly along the profile. Slightly higher velocities are determined for the deeper sediments of the asymmetric basin. This result can be explained by a higher compaction at the bottom of the basin due to the overburden. Otherwise, the two high-velocity layers within the sediments in domain D are characterized by velocities corresponding to evaporites (4.5–4.8 km/s) probably deposited during the Messinian event and commonly imaged in the Mediterranean basins (Gailler et al., 2009; Leprêtre et al., 2013). Based on the seismic velocities of these layers, an alternate hypothesis can be that they consist of carbonate deposits belonging to the Calabrian backstop. However, our preferred conclusion concerning these layers is that they are evaporitic sediments as interpreted previously from MCS data (Figures 5 and 6 of Polonia et al., 2016). As the evaporites were deposited in the deeper part of the basins, the absence of evaporites along most of the northern profile can be explained by its shallower bathymetrical position.

In domains A and D, the crustal thicknesses are modeled to be 29 and 26 km, respectively, and are characterized by low-velocity gradients indicating the presence of continental crust. They correspond to the Sicilian and the Calabrian continental domains. It can be observed that the upper crustal layer of the Calabrian domain is highly deformed (domain D). The slab roll-back may have deformed and fractured the crust in this region, which can explain the relatively low velocities in the upper crustal layer. The lack of information coming from the WAS on the lower crust of the Calabrian domain (D) do not allow us to extrapolate an origin for its velocities and thicknesses.

Based on the seismic velocities and geometry of the domain B, the Malta Escarpment is interpreted as a zone of abrupt crustal thinning. Its structure shares close similarity to other transform margins, especially very strong thinning over a lateral distance of only 40 km (see section 6.3; Mercier de Lépinay et al., 2016). Regarding the sedimentary basin edges, thinning at the Malta Escarpment is greater than along the Calabrian western edge but less steep (Figure 6, domains B and C). We propose that the Malta Escarpment is related to the original opening of the Tethys Ocean and the later influence of a STEP fault in this region, both of which will be discussed in more detail in a later section.

The crust located in domain C is interpreted as a two-layered thinned continental crust based on the low-velocity gradients and comparison to velocity-depth profiles from typical oceanic and continental crust (Figure 6) (Christensen & Mooney, 1995; White et al., 1992). But regarding only the internal velocities, the first layer of this crust could also be interpreted as a high-velocity sedimentary layer (Figure 6, green layer of domain D), similar to the one imaged on the southern profile (see section 6.2). Following this hypothesis, high amplitudes of reflected and refracted phases should be found in the next deeper interface as is generally observed at the interface between the sedimentary and the upper-crustal layers, which is not the case here. The major reflected and refracted phases are observed at the top of the high-velocity layer (from 5.0 to 5.4 km/s of the domain C) even if they are attenuated by the thickness of the overlying low-velocity layers (Figures 3a and 3b where the strong upper-crustal refraction corresponds to the continuity of this high-velocity layer). Moreover, in comparison to the southern high-velocity sedimentary layer, the northern one shows higher velocities (5.0–5.4 km/s to the north compared to 4.5 to 4.8 km/s to the south). These differences cannot be explained by the compaction of already lithified sediments. This layer shares more similarities, in terms of velocities, with the upper crust of the Calabrian continental domain D than with the Sicilian domain A. A less pronounced similarity is observed for the lower-crustal layer where the velocities and gradients of the thinned crust of domain C are more homogeneous in the Calabrian domain than the Sicilian (6.5 to 7.0 km/s for the Calabrian domain and the domain C rather than the 6.5 to 7.2 km/s for the Sicilian).

These observations are relevant for the interpretation of the origin of the basin and the identification of the major structures that limit the sedimentary basin on both sides. As discussed in the sections below, the high *P* wave velocity unit ($\geqslant$5 km thick) is interpreted to consist of Mesozoic carbonates. This layer is absent on the northern profile, and therefore, we conclude the deep asymmetrical basin opened in the Cenozoic. We propose that the basin was formed during the opening of the Messina Strait, between the Peloritan and the Calabrian terranes that are known to be diverging from GPS observations as well as major normal faulting earthquakes (Palano et al., 2012, 2017). While the Peloritan continental domain collides with the Nubian Sicily domain and therefore is locked, the Calabrian backstop is still free to continue its way to the south-east during slab roll-back. In between, a transtensional upper-plate basin opens following the thinning of the crust. In this hypothesis the edge of the Calabrian domain is interpreted as a major transtensional fault. This fault bounds the asymmetrical basin that formed in recent times.

The position of the oceanic crust that is subducting on the northern velocity profile is not constrained by our data. Two hypotheses can be proposed: the oceanic crust is already deep under the Calabrian backstop and a mantle layer separates them. In this hypothesis the WAS method could not reach the oceanic slab. The second hypothesis is that the oceanic crust cannot be observed in the velocity model because it cannot be resolved by our data set on the deeper eastern part. It may be located directly below the thin continental crust of the Calabrian block. But no evidence of such transition was found in our OBS data.

6.2. Interpretation of Profile DYP1

Along the southern DYP1 profile, the velocities and thickness of the sedimentary cover are more variable than along the northern profile. Along the Sicilian-Hyblean margin (domain E) two sedimentary layers are

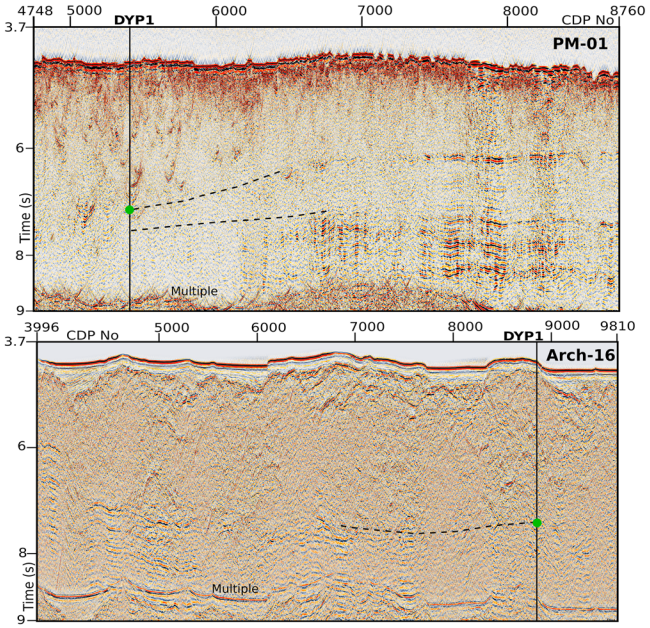

Figure 10. Multichannel seismic profiles crossing the southern DYP1 profile of this study, position marked in Figure 1. Top: PrisMed 01 (1993, R/V Le Nadir); bottom: Archimede (1997, R/V Le Nadir); processing is presented in Gallais et al. (2011). The green dots on crossing lines represent the top of the high velocity layer above the crust found on this study DYP1 profile. Notice that the lateral prolongation of this layer below the green dot shows a layered facies that is interpreted as high velocity sediments, likely deepwater carbonates.

characterized by relatively high sediment velocities (4.1–4.5 km/s) and are interpreted as thick layers of Mesozoic carbonates, as found in southern Sicily and on the Hyblean plateau (Monaco & De Guidi, 2006).

The uppermost sedimentary layer located within the basin (domains F, G, and H) is between 500 m and 3 km thick with relatively low velocities probably due to the high water content in this young sedimentary layer. Velocities and thicknesses are comparable to those modeled along the northern DYP3 profile. Underneath this layer, a sedimentary layer with higher velocities (4.3 km/s to 4.6 km/s) is imaged, likely corresponding to the Messinian evaporites as previously proposed (Gallais et al., 2011; Polonia et al., 2011, 2016). This layer presents a discontinuity in terms of seismic velocities with a low-velocity zone between 117 and 210 km of model offset. This zone is characterized by velocities similar to those found in the shallow sedimentary layers of the northern profile. We conclude that the pre-Messinian, clastic accretionary inner wedge (without high-velocity evaporites) is indenting the post-Messinian evaporitic wedge (Figure 1) as suggested by an earlier study (Gutscher et al., 2016). This interpretation of the WAS model is in good agreement with other geophysical data interpretations. For example, it is supported by the precedent analysis of the Messinian evaporite extent in the basin using seismic reflection data (Gallais et al., 2012). This indentation may also be correlated to observations in swath bathymetric data, such as several "slip-lines" that propagate through the post-Messinian wedge and originate from the southern termination of the AFS (Gutscher et al., 2017). Otherwise, the thickness of the evaporite layer increases from the foot of the Malta Escarpment and thins abruptly along the AFS at 117 km of offset along the profile. This observation indicates that the indentation postdates the formation of the Messinian evaporitic wedge. Also, on its western edge, the indentation seems to follow the AFS that probably acts as an inherited structure.

The deepest sedimentary layer has velocities similar to those of the evaporitic layer. However, the high velocities may be related to the nature of this layer and the compaction under the high overburden of 5–7 km of the upper sediments. Concerning its nature, as observed in previous studies, the velocities and velocity gradients of this layer are relatively difficult to model because of the overlying high-velocity evaporite layer and the velocity inversion (de Voogd et al., 1992; Makris et al., 1986; Nicolich et al., 2000). A comparison to existing reflection seismic studies shows that the corresponding seismic reflection facies is characterized by well-stratified reflections typical for sediments (Figure 10) (Catalano et al., 2001; Polonia et al., 2011, 2016). According to the MCS data this deep sedimentary layer seems to have been disturbed by the construction of the accretionary wedge.

The Sicilian crust (domain E of DYP1) is about 25–26 km thick and separated into two layers with velocities and velocity gradient characteristic for continental crust (Figure 7, domain E). This region belongs to the Hyblean plateau of the African plate and is similar to domain A of the northern profile DYP3. Direct comparison of both domains reveals that the lower crust of the northern profile is thicker than on the southern profile. This observation is probably related to the proximity of the Gela Nape thrust front on the northern DYP3 profile (Valenti et al., 2015). The deep structure of the Malta Escarpment (domain F) shows a similar width and geometry on both profiles, indicating that the margin has undergone a similar tectonic history in the north and south (Figure 7, domain F). We propose that it is a transition zone formed by the opening of a transform margin (see section 6.3).

The 8–10 km thick crust at the foot of the slope (domain G) is interpreted as a transitional crust that is more likely a thinned continental crust than a purely oceanic one. While the thickness might correspond to a thick oceanic crustal origin, the low-velocity gradients and the division into two layers of equal thickness support a thinned continental affinity (Figure 7, domain G). However, the possibility of a thick oceanic crust at this

location cannot be excluded. In this case, the crust could have been produced at the beginning of the oceanization of the basin, under thermal conditions that were different than for the rest of the profile. Our preferred interpretation is that domain G is underlain by thinned continental crust that was formed during the transform opening of the basin (Figure 7). This hypothesis is supported by the proximity of the Alfeo seamount, which is known to have a continental origin, because shallow-water carbonate sediments, similar to those of the Hyblean continental plateau, have been dredged here (Rossi & Borsetti, 1977).

Further to the east (domain H) the crust thins to 5–7 km thickness. It consists of a 2–3 km thick upper crustal layer and a 4 km thick lower crustal layer. The velocities in the lower crustal layer are significantly higher than in domain G. Comparison of the velocity-depth distribution functions from this domain to typical oceanic crust (White et al., 1992) and to serpentinised upper mantle material (Dean et al., 2000; Prada et al., 2014) shows that velocities here are untypical for both of these crustal types (Figure 7, domain H). The crust is slightly thinner than Atlantic type oceanic crust, and the velocities are slightly higher, especially the upper crustal layer. This might be related to its old age and compaction due to the thick overlying sedimentary layers. Otherwise, this could indicate that some peridotites have been incorporated into the crust probably at its formation, as can be observed at slow spreading ridges (Cannat, 1993; Sauter et al., 2013). The last hypothesis is in good agreement with earlier interpretations (D'Alessandro et al., 2016; Polonia et al., 2017); however, the diapiric structures presented in this latter study do not correspond to velocity anomalies along our profile, nor structures observed in the OBS data. Finally, the narrow transition zone between thinned continental crust and the oceanic domains corresponds to a deep expression of the AFS that seems to affect the entire crust (Nicolich et al., 2000). Altough the Moho depth and upper mantle velocities are less well constrained than the sedimentary and crustal structures, this part of the model is constrained by Pn and PmP arrivals (Figure 9).

6.3. Comparison With Other Continental Margins

To understand the origin of the Malta Escarpment and the Ionian basin, it is interesting to compare the deep structure of the eastern Sicily margin to other continental margins, formed by orthogonal rifting and oblique/transform rifting (Figure 11). Transform margins are mostly characterized by a narrow ocean-continent transition (OCT) zone and a short necking zone, on the order of 50–100 km, leading to a steep Moho inclination (Mercier de Lépinay et al., 2016, and references therein) (Figure 11, domains C and D). The zone over which crustal thinning occurs is about 50 km wide for the Demerara plateau in Guyana and 60 km in the Gulf of Cadiz (Greenroyd et al., 2008; Sallarès et al., 2011). Moreover, transform margins typically have a steep bathymetry with a strong continental slope angle (Mercier de Lépinay et al., 2016). On the contrary, orthogonal margins are characterized by a gentle continental slope and an OCT up to several hundreds of kilometers wide. For comparison the width of the crustal necking zone of the conjugate margin pair of Nova Scotia and Morocco is 150 to 250 km (Figure 11, domains A and B) (Biari et al., 2015; Funck et al., 2004).

Both final velocity models from our study (Figure 11, domains E and F) image a steep continental slope (13.2°) along the Malta Escarpment, which is also observed in the bathymetric data. The main thinning of the continental crust takes place over a short distance of about 50 km, although on the northern profile oceanization never sets in because it was already being subducted and cut by the Calabrian backstop. This leads us to conclude that the deep structure of the Malta Escarpment is an abrupt crustal necking zone, and in comparison to other margins, the eastern Sicily margin exhibits the typical characteristics of transform margins. This conclusion has geodynamic implications concerning the mechanism of the formation of the Ionian basin and leads us to propose that the basin was formed in a transform margin setting during the Early Mesozoic as was proposed earlier (Frizon de Lamotte et al., 2011; Gallais et al., 2011). In this interpretation the Apulian Escarpment cannot be considered as a conjugate margin of the Malta Escarpment.

6.4. Location of the Proposed STEP Fault

The most probable location for the major lithospheric tear (or STEP) fault can be deduced from the velocity models, as this major fault will affect the entire crust reaching into the upper mantle. The STEP fault in the Ionian basin has been active since the last 8–10 Ma (Gallais et al., 2013; Polonia et al., 2016). The sense of motion along the STEP fault has to be normal in the southern part of the basin, due to the collapse of the subducting plate, and strike-slip motion will occur additionally to the normal one in the northern part because of the upper plate advance in response to slab-roll back (Gallais et al., 2013). For these reasons,

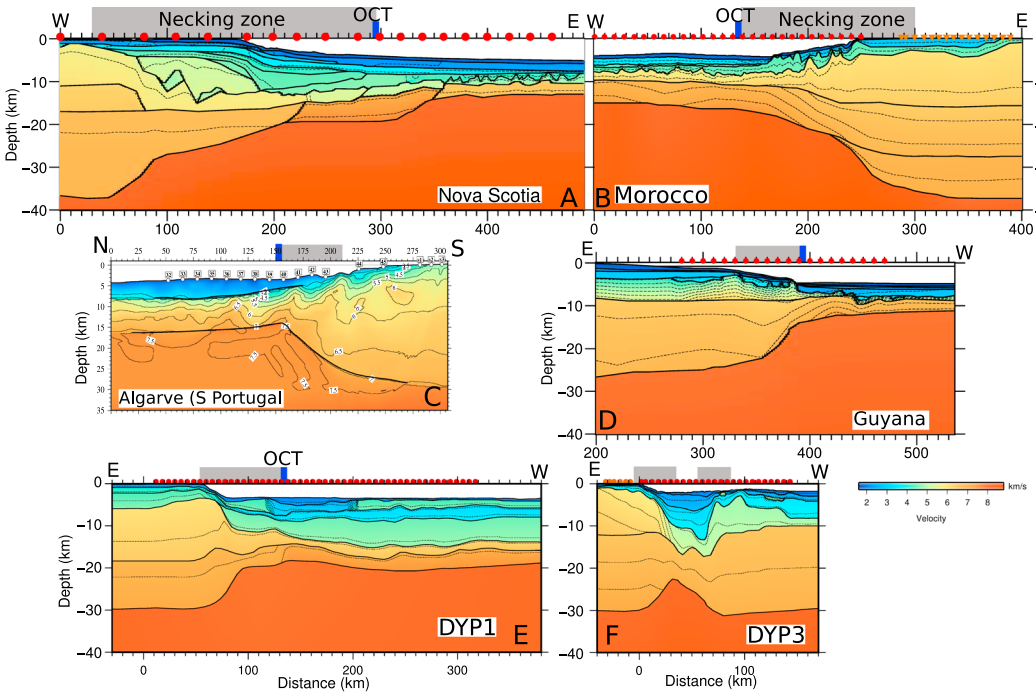

Figure 11. Comparison of velocity models at the same scale (VE = 4) from two known orthogonallu rifted margins (A and B), two known transform margins (C and D), and from this study (E and F). Morocco profile (Biari et al., 2015), Nova Scotia (Funck et al., 2004), Guyana (Greenroyd et al., 2008), and Gulf of Cadiz are from a tomographic inversion (Sallarès et al., 2011), while the others use a forward modeling approach). The gray rectangles represent the necking zone, and the blue triangle marks the ocean-continent transition.

three hypotheses prevail for the STEP fault location: the Malta Escarpment (Argnani & Bonazzi, 2005), the AFS (Gutscher et al., 2016), and the IFS (Polonia et al., 2016). Our two velocity models trend perpendicular to the three structures and thus allow us to verify to what extent the structures affect the crust.

The first hypothesis places the STEP fault along the foot of the Malta Escarpment because it is the major bathymetric feature and active normal faults were observed at its foot (Argnani & Bonazzi, 2005). According to our study, the Malta escarpment affects the crust, which thins from 29 to only 8 km. However, as explained above, this structure is mainly inherited from the original margin formation in the Early Mesozoic. Previous studies conclude that the activity along the escarpment is mostly normal and is closely related to its own collapse (Torelli et al., 1998) and in the northern part to the collapse of the eastern flank of the Mount Etna. Moreover, the presence of a thinned continental domain observed at the foot of the escarpment (domain G) cannot be explained without invoking a major deformation zone with a crustal expression, which is observed at the AFS.

This is why the second hypothesis places the tear fault along the AFS. Along this deformation structure, the faulting is mainly normal in the southern part of the basin developing a shear component closer to the backstop boundary in the north, as was observed in bathymetry and shallow seismic reflection profiles (Gallais et al., 2013; Gutscher et al., 2016). The final velocity model DYP1 images a lateral change of sedimentary velocities as well as the transition from thinned continental crust to oceanic crust at the location the AFS. The indentation caused by the advance of the clastic inner wedge through the evaporitic wedge coincides with the transition between the thinned continental and the oceanic crustal domains. Moreover, this structure affects the crust down to Moho depth in the southern velocity model, as also observed in reflection seismic data (Nicolich et al., 2000).

The third hypothesis proposes that the location of the STEP fault trends along the IFS. On the southern DYP1 velocity model the oceanic crust present throughout the eastern portion of the profile does not appear to be disturbed (thinned or thickened) at the location of the IFS. A decrease of the upper-crust over lower-crust

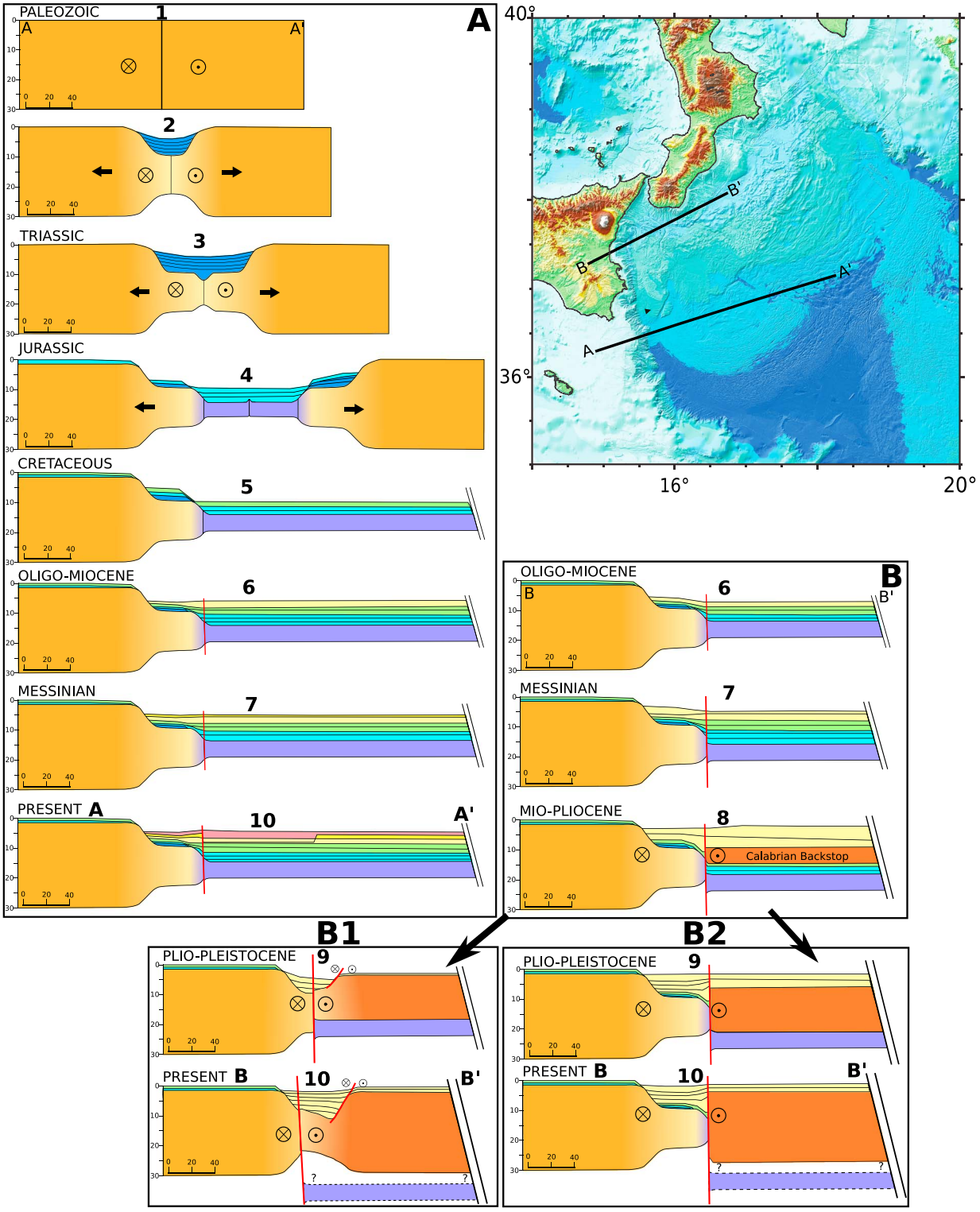

Figure 12. Proposed simplified tectonic evolution of the margins structures. A: Long term evolution of the eastern Sicily margin corresponding to the southern DYP1 profile. B 1 and B2: Long-term evolution of the Northern part of the eastern Sicily margin corresponding to the DYP3 profile including a recent collision phase. Please notice that before the Oligo-Miocene (step 6), the margins along both profiles have the same evolution. B1: First hypothesis that places the STEP fault along the Ionian fault system. Notice the presence of a Jurassic-Cretaceous sediment layer at the bottom of the basin. B2: Second hypothesis with the STEP fault placed along the Alfeo Fault System. Note the absence of the Jurassic-Cretaceous sediments and the thicker crust. In this last hypothesis the basin find its origin in rifting of the Calabrian and Peloritan continental terranes. The relative movements of blocks in the plan are represented by the cross and point symbols.

thickness ratio is observed, but the resolution of the model at this location is poorer than for the rest of the profile. Although the STEP fault is more difficult to identify along the northern DYP3 profile, a major fault at the flank of the Calabrian continental domain can explain the deep and asymmetric sedimentary basin observed along the profile. This structure appears to correspond closely to the deep expression of the IFS in its northern part. It seems logical to place the STEP fault along this major structure at the location of the northern velocity model because of its crustal expression and already known associated faults (Polonia et al., 2011, 2016). However, if the STEP fault location is along the IFS, then the margin observed in the north would be the same as the undeformed margin observed in the south, especially domains C and G should be similar (Figure 12, domain B2). The Calabrian backstop in response to slab roll-back advances toward the south-east and comes from behind the cross section. As the oceanic domain is subducted, a new limit along the ancient OCT is created. It is important to notice that the thick layer of high-velocity sediments should be observed in the northern velocity model similar to the southern model and that the asymmetry of the basin is more difficult to explain in such a scenario.

The observations drawn from the velocity models of this study include the following: (1) the deep structure of the Malta Escarpment is different on both profiles, especially in domains C and G, (2) the deep high-velocity sedimentary layer is absent on the northern profile, and (3) the thinned continental crust found at the bottom of the domain C shows a greater affinity to the Calabrian backstop than the Sicilian one. Therefore, we propose that the IFS results from the opening of the deep asymmetrical sedimentary basin that found its origin in the collision of the Peloritan with Nubian Sicily and its separation of the Calabrian block (Figure 12, domain B1). We propose that the thinned continental crust observed on domain C belongs to the Calabrian-Peloritan domains. The limit observed at 20 km of model offset in the northern velocity model is in good agreement with this hypothesis, where the thinned continental domain of the Calabrian-Peloritan terranes collides with the Sicilian one. In this case, the most probable location for the STEP fault on both velocity models is the AFS as was previously proposed (Gallais et al., 2013; Gutscher et al., 2016). The STEP fault on the northern velocity model is placed at 20 to 30 km of model offset. In this hypothesis the structure limits the Sicilian Nubian domain to the west and the Peloritan-Calabrian thinned continental domain to the east.

Finally, this hypothesis is in good agreement with onshore observations as the prolongation of the AFS follows the geological transition of the Taormina line that limits the Nubian plate and the Peloritan continental block. Moreover, the presence of Mount Etna along this direction, and the geochemical nature of its extrusive volcanic rocks, which indicates a deep-mantle origin of the volcano, also supports this location for the STEP fault (Schiano et al., 2001).

7. Conclusions

The WAS data acquired during the DIONYSUS survey image the deep structure of the Ionian basin and the eastern Sicily margin. The crust observed in the deeper parts of the basin (DYP1) has strong similarities in terms of velocities and gradients with an oceanic-type crust. But the hypothesis of a peridotites intruded oceanic crust or partially serpentinized upper mantle cannot be excluded. The Malta Escarpment is imaged as a zone of abrupt crustal thinning extending 50–60 km further east of its bathymetric expression. As its structure is highly similar to other transform margins it likely represents a remnant of a transform margin that formed during the Early Mesozoic. According to our results and preceding works in the area, we believe that the Ionian basin can be considered as a remnant of the Neo-Tethys ocean.

Concerning the recent geodynamic history of the basin and especially the lithospheric tear fault location, we favor the hypothesis that the STEP fault follows the trend of the AFS rather than the Malta Escarpment or the IFS. This conclusion is based on several arguments that correspond to earlier results corroborated by the new velocity models. The first argument concerns the southern profile DYP1, where the AFS affects the crust down to the crust-mantle boundary and is located along a transition between a thinned continental domain and an oceanic one. Also, according to recent MCS data, the AFS is still active today with normal to transcurrent motion along its southern extension and dextral strike-slip motion to the north (Gallais et al., 2013; Gutscher et al., 2016; with high-resolution seismic profiles). The second is that, on the contrary, the IFS does not affect the crust in our velocity model, even if it is an active structure close to the Calabrian block. Finally, the Malta escarpment affects the crust but does not seem to be an active strike-slip tectonic feature, as its faults correspond to a normal motion that can be related to its own collapse. Our conclusion for the tear

fault location in the northern profile is that this recent structure is probably superposed to the ancient structure of the Malta escarpment. The location of the subducting slab along the northern profile remains an open question that will be explored in the future using a 3-D gravity modeling.

Acknowledgments
We thank the captain and crew of the R/V Meteor for the data acquisition during the marine survey. The DIONYSUS cruise is funded through the Deutsche Forschungsgemeinschaft DFG. We also acknowledge *Région Bretagne* and Ifremer for funding the PhD scholarship associated to this work, as well as the University of Western Brittany (UBO) and the LabexMer for their help and funding of this work. We would like to acknowledge scientists and technical teams of the INGV for deploying the land stations and Bruno Marsset from Ifremer for help processing these data. Most of the figures from this paper were generated using the Generic Mapping Tools version 4.5.8 (http://gmt.soest.hawaii.edu), and the SU (Seismic Unix) software was used for processing the WAS data as well as calculation of the synthetic data (Cohen & Stockwell, 2003). We would like to thank Alina Polonia for providing access to the CROP-M3 profile, coincident to the DYP1 profile of this study. We would like to thank the reviewers Sara Martínez-Loriente and Manel Prada that provided constructive comments, which helped in the revision of the manuscript. The raw data used in this publication are accessible on demand at http://doi.org/10.17882/52435.

References

Agard, P., Omrani, J., Jolivet, L., Whitechurch, H., Vrielynck, B., Spakman, W., et al. (2011). Zagros orogeny: A subduction-dominated process. *Geological Magazine*, *148*(5-6), 692–725. https://doi.org/10.1017/S001675681100046X

Amato, A., Alessandrini, B., Cimini, G., Frepoli, A., & Selvaggi, G. (1993). Active and remnant subducted slabs beneath Italy: Evidence from seismic tomography. *Annali di Geofisica*, *36*(2), 201–214.

Argnani, A. (2009). Evolution of the southern Tyrrhenian slab tear and active tectonics along the western edge of the Tyrrhenian subducted slab. *Geological Society, London, Special Publications*, *311*(1), 193–212.

Argnani, A., & Bonazzi, C. (2005). Malta Escarpment fault zone offshore eastern Sicily: Pliocene-Quaternary tectonic evolution based on new multichannel seismic data: Offshore eastern Sicily. *Tectonics*, *24*, TC4009. https://doi.org/10.1029/2004TC001656

Argnani, A., Cimini, G. B., Frugoni, F., Monna, S., & Montuori, C. (2016). The role of continental margins in the final stages of arc formation: Constraints from teleseismic tomography of the Gibraltar and Calabrian Arc (western Mediterranean). *Tectonophysics*, *677-678*, 135–152. https://doi.org/10.1016/j.tecto.2016.03.037

Auffret, Y., Pelleau, P., Klingelhoefer, F., Geli, L., Crozon, J., Lin, J. Y., & Sibuet, J.-C. (2004). MicrOBS: A new generation of ocean bottom seismometer. *First Break*, *22*, 41–47.

Baccheschi, P., Margheriti, L., Steckler, M. S., & Boschi, E. (2011). Anisotropy patterns in the subducting lithosphere and in the mantle wedge: A case study–The southern Italy subduction system. *Journal of Geophysical Research*, *116*, B08306. https://doi.org/10.1029/2010JB007961

Bialas, J., & Flueh, E. R. (1999). Ocean bottom seismometers. *Sea Technology*, *40*, 41–46.

Biari, Y., Klingelhoefer, F., Sahabi, M., Aslanian, D., Schnurle, P., Berglar, K., et al. (2015). Deep crustal structure of the North-West African margin from combined wide-angle and reflection seismic data (MIRROR seismic survey). *Tectonophysics*, *656*, 154–174. https://doi.org/10.1016/j.tecto.2015.06.019

Bonvalot, S., Balmino, G., Briais, A., Kuhn, M., Peyrefitte, A., Vales N., et al. (2012). World gravity map. *Commission for the Geological Map of the World*. Eds. BGI-CGMW-CNES-IRD, Paris.

Bouillin, J. P. (1986). Le "bassin maghrebin"; une ancienne limite entre l'Europe et l'Afrique a l'ouest des Alpes. *Bulletin de la Société géologique de France*, *2*(4), 547–558.

Cannat, M. (1993). Emplacement of mantle rocks in the seafloor at mid ocean ridges. *Journal of Geophysical Research*, *98*(B3), 4163–4172. https://doi.org/10.1029/92JB02221

Catalano, R., Doglioni, C., & Merlini, S. (2001). On the Mesozoic Ionian basin. *Geophysical Journal International*, *144*(1), 49–64. https://doi.org/10.1046/j.0956-540X.2000.01287.x

Cernobori, L., Hirn, A., McBride, J. H., Nicolich, R., Petronio, L., Romanelli, M., & Streamers/Profiles Working Groups (1996). Crustal image of the Ionian basin and its Calabrian margins. *Tectonophysics*, *264*(1-4), 175–189. https://doi.org/10.1016/S0040-1951(96)00125-4

Chiarabba, C., De Gori, P., & Speranza, F. (2008). The southern Tyrrhenian subduction zone: Deep geometry, magmatism and Plio-Pleistocene evolution. *Earth and Planetary Science Letters*, *268*(3-4), 408–423. https://doi.org/10.1016/j.epsl.2008.01.036

Chiarabba, C., & Palano, M. (2017). Progressive migration of slab break-off along the southern Tyrrhenian plate boundary: Constraints for the present day kinematics. *Journal of Geodynamics*, *105*, 51–61. https://doi.org/10.1016/j.jog.2017.01.006

Chiocci, F. L., Coltelli, M., Bosman, A., & Cavallaro, D. (2011). Continental margin large-scale instability controlling the flank sliding of Etna volcano. *Earth and Planetary Science Letters*, *305*(1-2), 57–64. https://doi.org/10.1016/j.epsl.2011.02.040

Christensen, N. I., & Mooney, W. D. (1995). Seismic velocity structure and composition of the continental crust: A global view. *Journal of Geophysical Research*, *100*(B6), 9761–9788. https://doi.org/10.1029/95JB00259

Cimini, G. B. (1999). P-wave deep velocity structure of the southern Tyrrhenian Subduction Zone from nonlinear teleseismic travel-time tomography. *Geophysical Research Letters*, *26*(24), 3709–3712. https://doi.org/10.1029/1999GL010907

Civello, S., & Margheriti, L. (2004). Toroidal mantle flow around the Calabrian slab (Italy) from SKS splitting. *Geophysical Research Letters*, *31*, L10601. https://doi.org/10.1029/2004GL019607

Cohen, J. K., & Stockwell, J. W. Jr. (2003). CWP/SU: Seismic Unix release no. 36: A free package for seismic research and processing. Center for Wave Phenomena, Colorado School of Mines.

D'Agostino, N., D'Anastasio, E., Gervasi, A., Guerra, I., Nedimović, M. R., Seeber, L., & Steckler, M. (2011). Forearc extension and slow rollback of the Calabrian Arc from GPS measurements: Forearc extension of the Calabrian arc. *Geophysical Research Letters*, *38*, L17304. https://doi.org/10.1029/2011GL048270

D'Alessandro, A., Mangano, G., D'Anna, G., & Scudero, S. (2016). Evidence for serpentinization of the Ionian upper mantle from simultaneous inversion of P-and S-wave arrival times. *Journal of Geodynamics*, *102*, 115–120. https://doi.org/10.1016/j.jog.2016.09.003

de Voogd, B., Truffert, C., Chamot Rooke, N., Huchon, P., Lallemant, S., & Pichon, X. (1992). Two ship deep seismic soundings in the basins of the eastern Mediterranean Sea (Pasiphae cruise). *Geophysical Journal International*, *109*(3), 536–552. https://doi.org/10.1111/j.1365-246X.1992.tb00116.x

Dean, S. M., Minshull, T. A., Whitmarsh, R. B., & Louden, K. E. (2000). Deep structure of the ocean continent transition in the southern Iberia Abyssal Plain from seismic refraction profiles: The IAM 9 transect at 40 20′N. *Journal of Geophysical Research*, *105*(B3), 5859–5885. https://doi.org/10.1029/1999JB900301

Della Vedova, B., Pellis, G., & Pinna, E. (1989). Studio geofisico dell'area di transizione tra il Mar Pelagico e la Piana Abissale dello Jonio. *Atti dell'8° Convegno del Gruppo Nazionale di Geofisica della Terra Solida, Roma*, *1*, 543–558.

Dercourt, J., Zonenshain, L. P., Ricou, L.-E., Kazmin, V. G., Le Pichon, X., Knipper, A. L., et al. (1986). Geological evolution of the Tethys belt from the Atlantic to the Pamirs since the Lias. *Tectonophysics*, *123*(1-4), 241–315. https://doi.org/10.1016/0040-1951(86)90199-X

Dewey, J. F., Helman, M. L., Knott, S. D., Turco, E., & Hutton, D. H. W. (1989). Kinematics of the western Mediterranean. *Geological Society, London, Special Publications*, *45*(1), 265–283. https://doi.org/10.1144/GSL.SP.1989.045.01.15

Faccenna, C., Becker, T. W., Lucente, F. P., Jolivet, L., & Rossetti, F. (2001). History of subduction and back arc extension in the Central Mediterranean. *Geophysical Journal International*, *145*(3), 809–820. https://doi.org/10.1046/j.0956-540x.2001.01435.x

Finetti, I. (1982). Structure, stratigraphy and evolution of central Mediterranean. *Bollettino di Geofisica Teorica ed Applicata*, *24*(96), 247–312.

Frizon de Lamotte, D., Raulin, C., Mouchot, N., Wrobel-Daveau, J.-C., Blanpied, C., & Ringenbach, J.-C. (2011). The southernmost margin of the Tethys realm during the Mesozoic and Cenozoic: Initial geometry and timing of the inversion processes: Tethys southernmost margin. *Tectonics*, *30*, TC3002. https://doi.org/10.1029/2010TC002691

Funck, T., Jackson, H. R., Louden, K. E., Dehler, S. A., & Wu, Y. (2004). Crustal structure of the northern Nova Scotia rifted continental margin (eastern Canada): Structure of Nova Scotia rifted margin. *Journal of Geophysical Research*, *109*, B09102. https://doi.org/10.1029/2004JB003008

Gailler, A., Klingelhoefer, F., Olivet, J. L., Aslanian, D., Sardinia Sci, P., & Tech, O. B. S. T. (2009). Crustal structure of a young margin pair: New results across the Liguro-Provencal basin from wide- angle seismic tomography. *Earth and Planetary Science Letters*, *286*(1-2), 333–345. https://doi.org/10.1016/j.epsl.2009.07.001

Gallais, F., Graindorge, D., Gutscher, M.-A., & Klaeschen, D. (2013). Propagation of a lithospheric tear fault (STEP) through the western boundary of the Calabrian accretionary wedge offshore eastern Sicily (southern Italy). *Tectonophysics*, *602*, 141–152. https://doi.org/10.1016/j.tecto.2012.12.026

Gallais, F., Gutscher, M.-A., Graindorge, D., Chamot-Rooke, N., & Klaeschen, D. (2011). A Miocene tectonic inversion in the Ionian Sea (central Mediterranean): Evidence from multichannel seismic data. *Journal of Geophysical Research*, *116*, B12108. https://doi.org/10.1029/2011JB008505

Gallais, F., Gutscher, M.-A., Klaeschen, D., & Graindorge, D. (2012). Two-stage growth of the Calabrian accretionary wedge in the Ionian Sea (Central Mediterranean): Constraints from depth migrated multichannel seismic data. *Marine Geology*, *326-328*, 28–45. https://doi.org/10.1016/j.margeo.2012.08.006

Govers, R., & Wortel, M. J. R. (2005). Lithosphere tearing at STEP faults: Response to edges of subduction zones. *Earth and Planetary Science Letters*, *236*(1-2), 505–523. https://doi.org/10.1016/j.epsl.2005.03.022

Greenroyd, C. J., Peirce, C., Rodger, M., Watts, A. B., & Hobbs, R. W. (2008). Demerara Plateau—The structure and evolution of a transform passive margin. *Geophysical Journal International*, *172*(2), 549–564. https://doi.org/10.1111/j.1365-246X.2007.03662.x

Gross, F., Krastel, S., Geersen, J., Behrmann, J. H., Ridente, D., Chiocci, F. L., et al. (2016). The limits of seaward spreading and slope instability at the continental margin offshore Mt Etna, imaged by high-resolution 2D seismic data. *Tectonophysics*, *667*, 63–76.

Gutscher, M.-A., Dominguez, S., de Lepinay, B. M., Pinheiro, L., Gallais, F., Babonneau, N., et al. (2016). Tectonic expression of an active slab tear from high-resolution seismic and bathymetric data offshore Sicily (Ionian Sea). *Tectonics*, *35*, 39–54. https://doi.org/10.1002/2015TC003898

Gutscher, M.-A., Kopp, H., Krastel, S., Bohrmann, G., Garlan, T., Zaragosi, S., et al. (2017). Active tectonics of the Calabrian subduction revealed by new multi-beam bathymetric data and high-resolution seismic profiles in the Ionian Sea (Central Mediterranean). *Earth and Planetary Science Letters*, *461*, 61–72. https://doi.org/10.1016/j.epsl.2016.12.020

Hirn, A., Nicolich, R., Gallart, J., Laigle, M., Cernobori, L., & Group, ES (1997). Roots of Etna volcano in faults of great earthquakes. *Earth and Planetary Science Letters*, *148*(1-2), 171–191. https://doi.org/10.1016/S0012-821X(97)00023-X

Jolivet, L., Faccenna, C., Agard, P., Frizon de Lamotte, D., Menant, A., Sternai, P., & Guillocheau, F. (2015). Neo-Tethys geodynamics and mantle convection: From extension to compression in Africa and a conceptual model for obduction. *Canadian Journal of Earth Sciences*, *53*(11), 1190–1204.

Lallemand, S., & Funiciello, F. (Eds.) (2009). *Subduction zone geodynamics, Frontiers in Earth Sciences*. Berlin: Springer. https://doi.org/10.1007/978-3-540-87974-9

Le Meur, D. (1997). Etude géophysique de la structure profonde et de la tectonique active de la partie occidentale de la Ride Méditerranéenne (*Doctoral dissertation*).

Leprêtre, A., Klingelhoefer, F., Graindorge, D., Schnurle, P., Beslier, M. O., Yelles, K., et al. (2013). Multiphased tectonic evolution of the Central Algerian margin from combined wide-angle and reflection seismic data off Tipaza, Algeria. *Journal of Geophysical Research: Solid Earth*, *118*, 3899–3916. https://doi.org/10.1002/jgrb.50318

Lonergan, L., & White, N. (1997). Origin of the Betic Rif mountain belt. *Tectonics*, *16*(3), 504–522. https://doi.org/10.1029/96TC03937

Loureiro, A., Afilhado, A., Matias, L., Moulin, M., & Aslanian, D. (2016). Monte Carlo approach to assess the uncertainty of wide-angle layered models: Application to the Santos Basin, Brazil. *Tectonophysics*, *683*, 286–307. https://doi.org/10.1016/j.tecto.2016.05.040

Ludwig, W. J., Nafe, J. E., & Drake, C. L. (1970). Seismic refraction. *The sea*, *4*(part 1), 53–84.

Makris, J., Nicolich, R., & Weigel, W. (1986). A seismic study in the western Ionian Sea. In Annales geophysicae. *Series B. Terrestrial and Planetary Physics*, *4*(6), 665–678.

Malinverno, A., & Ryan, W. B. (1986). Extension in the Tyrrhenian Sea and shortening in the Apennines as result of arc migration driven by sinking of the lithosphere. *Tectonics*, *5*(2), 227–245. https://doi.org/10.1029/TC005i002p00227

Mercier de Lépinay, M., Loncke, L., Basile, C., Roest, W. R., Patriat, M., Maillard, A., & De Clarens, P. (2016). Transform continental margins—Part 2: A worldwide review. *Tectonophysics*, *693*, 96–115. https://doi.org/10.1016/j.tecto.2016.05.038

Minelli, L., & Faccenna, C. (2010). Evolution of the Calabrian accretionary wedge (central Mediterranean): Calabrian accretionary wedge. *Tectonics*, *29*, TC4004. https://doi.org/10.1029/2009TC002562

Monaco, C., & De Guidi, G. (2006). Structural evidence for Neogene rotations in the eastern Sicilian fold and thrust belt. *Journal of Structural Geology*, *28*(4), 561–574. https://doi.org/10.1016/j.jsg.2006.01.010

Moretti, M., Improta, L., Margheriti, L., De Gori, P., Silvestri, M., Criscuoli, F., et al. (2015). Esperimento DIONYSUS: Deep structure of the IONian Sea and east SicilY: Wide-angle seismic SUrvey of the Calabria Subduction zone and Tethys margins. Il contributo dell'Istituto Nazionale di Geofisica e Vulcanologia. *Rapporti Tecnini INGV*.

Neri, G., Marotta, A. M., Orecchio, B., Presti, D., Totaro, C., Barzaghi, R., & Borghi, A. (2012). How lithospheric subduction changes along the Calabrian Arc in southern Italy: Geophysical evidences. *International Journal of Earth Sciences*, *101*(7), 1949–1969. https://doi.org/10.1007/s00531-012-0762-7

Neri, G., Orecchio, B., Totaro, C., Falcone, G., & Presti, D. (2009). Subduction beneath southern Italy close the ending: Results from seismic tomography. *Seismological Research Letters*, *80*(1), 63–70. https://doi.org/10.1785/gssrl.80.1.63

Nicolich, R., Laigle, M., Hirn, A., Cernobori, L., & Gallart, J. (2000). Crustal structure of the Ionian margin of Sicily: Etna volcano in the frame of regional evolution. *Tectonophysics*, *329*(1-4), 121–139. https://doi.org/10.1016/S0040-1951(00)00192-X

Orecchio, B., Presti, D., Totaro, C., D'Amico, S., & Neri, G. (2015). Investigating slab edge kinematics through seismological data: The northern boundary of the Ionian subduction system (south Italy). *Journal of Geodynamics*, *88*, 23–35. https://doi.org/10.1016/j.jog.2015.04.003

Palano, M. (2016). Episodic slow slip events and seaward flank motion at Mt. Etna volcano (Italy). *Journal of Volcanology and Geothermal Research*, *324*, 8–14. https://doi.org/10.1016/j.jvolgeores.2016.05.010

Palano, M., Ferranti, L., Monaco, C., Mattia, M., Aloisi, M., Bruno, V., et al. (2012). GPS velocity and strain fields in Sicily and southern Calabria, Italy: Updated geodetic constraints on tectonic block interaction in the central Mediterranean: GPS velocity/strain in south Italy. *Journal of Geophysical Research*, *117*, B07401. https://doi.org/10.1029/2012JB009254

Palano, M., Piromallo, C., & Chiarabba, C. (2017). Surface imprint of toroidal flow at retreating slab edges: The first geodetic evidence in the Calabrian subduction system: Surface imprint of toroidal flow. *Geophysical Research Letters*, *44*, 845–853. https://doi.org/10.1002/2016GL071452

Piromallo, C., & Morelli, A. (2003). P wave tomography of the mantle under the Alpine-Mediterranean area. *Journal of Geophysical Research*, *108*(B2), 2065. https://doi.org/10.1029/2002JB001757

Polonia, A., Torelli, L., Artoni, A., Carlini, M., Faccenna, C., Ferranti, L., et al. (2016). The Ionian and Alfeo–Etna fault zones: New segments of an evolving plate boundary in the central Mediterranean Sea? *Tectonophysics*, *675*, 69–90. https://doi.org/10.1016/j.tecto.2016.03.016

Polonia, A., Torelli, L., Gasperini, L., Cocchi, L., Muccini, F., Bonatti, E., et al. (2017). Lower plate serpentinite diapirism in the Calabrian Arc subduction complex. *Nature Communications*, *8*(1), 2172. https://doi.org/10.1038/s41467-017-02273-x

Polonia, A., Torelli, L., Mussoni, P., Gasperini, L., Artoni, A., & Klaeschen, D. (2011). The Calabrian Arc subduction complex in the Ionian Sea: Regional architecture, active deformation, and seismic hazard: The Calabrian arc subduction complex. *Tectonics*, *30*, TC5018. https://doi.org/10.1029/2010TC002821

Prada, M., Sallares, V., Ranero, C. R., Vendrell, M. G., Grevemeyer, I., Zitellini, N., & de Franco, R. (2015). The complex 3-D transition from continental crust to backarc magmatism and exhumed mantle in the Central Tyrrhenian basin. *Geophysical Journal International*, *203*(1), 63–78. https://doi.org/10.1093/gji/ggv271

Prada, M., Sallares, V., Ranero, C. R., Vendrell, M. G., Grevemeyer, I., Zitellini, N., & Franco, R. (2014). Seismic structure of the Central Tyrrhenian basin: Geophysical constraints on the nature of the main crustal domains. *Journal of Geophysical Research. Solid Earth*, *119*, 52–70. https://doi.org/10.1002/2013JB010527

Prada, M., Sallares, V., Ranero, C. R., Vendrell, M. G., Grevemeyer, I., Zitellini, N., & Franco, R. (2016). Spatial variations of magmatic crustal accretion during the opening of the Tyrrhenian back-arc from wide-angle seismic velocity models and seismic reflection images. *Basin Research*, *30*, 124–141. https://doi.org/10.1111/bre.12211

Rehault, J.-P., Boillot, G., & Mauffret, A. (1984). The western Mediterranean basin geological evolution. *Marine Geology*, *55*(3-4), 447–477. https://doi.org/10.1016/0025-3227(84)90081-1

Ricou, L. E. (1994). Tethys reconstructed: Plates, continental fragments and their boundaries since 260 Ma from Central America to south-eastern Asia. *Geodinamica Acta*, *7*(4), 169–218. https://doi.org/10.1080/09853111.1994.11105266

Rosenbaum, G., Gasparon, M., Lucente, F. P., Peccerillo, A., & Miller, M. S. (2008). Kinematics of slab tear faults during subduction segmentation and implications for Italian magmatism: Kinematics of slab teat faults. *Tectonics*, *27*, TC2008. https://doi.org/10.1029/2007TC002143

Rosenbaum, G., Lister, G. S., & Duboz, C. (2002). Reconstruction of the tectonic evolution of the western Mediterranean since the Oligocene. *Journal of the Virtual Explorer*, *8*, 107–130.

Rossi, S., & Borsetti, A. M. (1977). Dati preliminari di stratigrafia e di sismica del mare Ionio settentrionale. *Memorie Società Geologica Italiana*, *13*, 251–259.

Roure, F., Casero, P., & Addoum, B. (2012). Alpine inversion of the north African margin and delamination of its continental lithosphere: Inversion of the north African margin. *Tectonics*, *31*, TC3006. https://doi.org/10.1029/2011TC002989

Sage, F., Pontoise, B., Mascle, J., & Basile, C. (1997). Structure of oceanic crust adjacent to a transform margin segment: The Côte d'Ivoire-Ghana transform margin. *Geo-Marine Letters*, *17*(1), 31–39. https://doi.org/10.1007/PL00007204

Sallarès, V., Gailler, A., Gutscher, M.-A., Graindorge, D., Bartolomé, R., Gràcia, E., et al. (2011). Seismic evidence for the presence of Jurassic oceanic crust in the central Gulf of Cadiz (SW Iberian margin). *Earth and Planetary Science Letters*, *311*(1-2), 112–123. https://doi.org/10.1016/j.epsl.2011.09.003

Sandwell, D. T., & Smith, W. H. F. (1997). Marine gravity anomaly from Geosat and ERS-1 satellite altimetry. *Journal of Geophysical Research*, *102*(B5), 10,039–10,054. https://doi.org/10.1029/96JB03223

Sauter, D., Cannat, M., Rouméjon, S., Andreani, M., Birot, D., Bronner, A., et al. (2013). Continuous exhumation of mantle-derived rocks at the Southwest Indian Ridge for 11 million years. *Nature Geoscience*, *6*, 314–320. https://doi.org/10.1038/ngeo1771

Schiano, P., Clocchiatti, R., Ottolini, L., & Busa, T. (2001). Transition of Mount Etna lavas from a mantle-plume to an island-arc magmatic source. *Nature*, *412*(6850), 900–904. https://doi.org/10.1038/35091056

Spakman, W., van der Lee, S., & van der Hilst, R. (1993). Travel-time tomography of the European-Mediterranean mantle down to 1400 km. *Physics of the Earth and Planetary Interiors*, *79*(1-2), 3–74. https://doi.org/10.1016/0031-9201(93)90142-V

Spakman, W., & Wortel, R. (2004). A tomographic view on western Mediterranean geodynamics. In W. Cavazza, et al. (Eds.), *The TRANSMED Atlas. The Mediterranean Region from crust to mantle* (pp. 31–52). Berlin: Springer.

Speranza, F., Minelli, L., Pignatelli, A., & Chiappini, M. (2012). The Ionian Sea: The oldest in situ ocean fragment of the world?: Magnetic modelling of the Ionian sea. *Journal of Geophysical Research*, *117*, B12101. https://doi.org/10.1029/2012JB009475

Stampfli, G. M., & Borel, G. D. (2004). The TRANSMED transects in space and time: Constraints on the paleotectonic evolution of the Mediterranean domain. In W. Cavazza, et al. (Eds.), *The TRANSMED Atlas. The Mediterranean Region from crust to mantle* (pp. 53–80). Berlin: Springer.

Stampfli, G. M., Borel, G. D., Marchant, R., & Mosar, J. (2002). Western Alps geological constraints on western Tethyan reconstructions. *Journal of the Virtual Explorer*, *8*, 77.

Stockwell, D. R. B. (1999). Genetic algorithms II. In A. H. Fielding (Ed.), *Machine learning methods for ecological applications* (pp. 123–144). Boston, MA: Kluwer Academic Publishers. https://doi.org/10.1007/978-1-4615-5289-5_5

Stockwell, J. W., & Cohen, J. K. (2003). The CWP/SU: Seismic Unix release 37: A free package for seismic research and processing. Center for Wave Phenomena, Colorado School of Mines.

Torelli, L., Grasso, M., Mazzoldi, G., & Peis, D. (1998). Plio–Quaternary tectonic evolution and structure of the Catania foredeep, the northern Hyblean Plateau and the Ionian shelf (SE Sicily). *Tectonophysics*, *298*(1-3), 209–221. https://doi.org/10.1016/S0040-1951(98)00185-1

Trippetta, F., Collettini, C., Vinciguerra, S., & Meredith, P. G. (2010). Laboratory measurements of the physical properties of Triassic Evaporites from Central Italy and correlation with geophysical data. *Tectonophysics*, *492*(1-4), 121–132. https://doi.org/10.1016/j.tecto.2010.06.001

Valenti, V., Catalano, R., Wei, P., & Wang, S. (2015). Layered lower crust and mantle reflectivity as imaged by a re-processed crustal seismic profile from Sicily in the central Mediterranean. *Bulletin de la Société Géologique de France*, *186*(4-5), 257–272. https://doi.org/10.2113/gssgfbull.186.4-5.257

van Hinsbergen, D. J. J., Vissers, R. L. M., & Spakman, W. (2014). Origin and consequences of western Mediterranean subduction, rollback, and slab segmentation: Western Mediterranean subduction. *Tectonics*, *33*, 393–419. https://doi.org/10.1002/2013TC003349

White, R. S., McKenzie, D., & O'Nions, R. K. (1992). Oceanic crustal thickness from seismic measurements and rare earth element inversions. *Journal of Geophysical Research*, *97*(B13), 19,683–19,715. https://doi.org/10.1029/92JB01749

Wildi, W. (1983). La chaîne tello-rifaine (Algérie, Maroc, Tunisie): Structure, stratigraphie et évolution du Trias au Miocène. *Revue de Géographie Physique et de Géologie Dynamique*, *24*(3), 201–297.

Wortel, R., Govers, R., & Spakman, W. (2009). Continental collision and the STEP-wise evolution of convergent plate boundaries: From structure to dynamics. *Subduction Zone Geodynamics*, *47-59*. https://doi.org/10.1007/978-3-540-87974-9_3

Zelt, C. A. (1999). Modelling strategies and model assessment for wide-angle seismic travel-time data. *Geophysical Journal International*, *139*(1), 183–204. https://doi.org/10.1046/j.1365-246X.1999.00934.x

Zelt, C. A., & Smith, R. B. (1992). Seismic travel-time inversion for 2-D crustal velocity structure. *Geophysical Journal International*, *108*(16–34), 1992.